Available online at www.sciencedirect.com
SCIENCE DIRECT
Neurochemistry International 44 (2004) 497–503
NEUROCHEMISTRY International
www.elsevier.com/locate/neuint

Simultaneous monitoring of acetylcholine and catecholamine release in the in vivo rat adrenal medulla

Tsuyoshi Akiyama[a,*], Toji Yamazaki[a], Hidezo Mori[a], Kenji Sunagawa[b]

[a] *Department of Cardiac Physiology, National Cardiovascular Center Research Institute, 5-7-1 Fujishiro-dai, Suita, Osaka 565-8565, Japan*
[b] *Department of Cardiovascular Dynamics, National Cardiovascular Center Research Institute, Suita, Osaka 565-8565, Japan*

Received 20 May 2003; accepted 3 September 2003

Abstract

To simultaneously monitor acetylcholine release from pre-ganglionic adrenal sympathetic nerve endings and catecholamine release from post-ganglionic adrenal chromaffin cells in the in vivo state, we applied microdialysis technique to anesthetized rats. Dialysis probe was implanted in the left adrenal medulla and perfused with Ringer's solution containing neostigmine (a cholinesterase inhibitor). After transection of splanchnic nerves, we electrically stimulated splanchnic nerves or locally administered acetylcholine through dialysis probes for 2 min and investigated dialysate acetylcholine, choline, norepinephrine and epinephrine responses. Acetylcholine was not detected in dialysate before nerve stimulation, but substantial acetylcholine was detected by nerve stimulation. In contrast, choline was detected in dialysate before stimulation, and dialysate choline concentration did not change with repetitive nerve stimulation. The estimated interstitial acetylcholine levels and dialysate catecholamine responses were almost identical between exogenous acetylcholine (10 μM) and nerve stimulation (2 Hz). Dialysate acetylcholine, norepinephrine and epinephrine responses were correlated with the frequencies of electrical nerve stimulation, and dialysate norepinephrine and epinephrine responses were quantitatively correlated with dialysate acetylcholine responses. Neither hexamethonium (a nicotinic receptor antagonist) nor atropine (a muscarinic receptor antagonist) affected the dialysate acetylcholine response to nerve stimulation. Microdialysis technique made it possible to simultaneously assess activities of pre-ganglionic adrenal sympathetic nerves and post-ganglionic adrenal chromaffin cells in the in vivo state and provided quantitative information about input–output relationship in the adrenal medulla.

Keywords: Anesthetized rats; Microdialysis; Choline; Norepinephrine; Epinephrine

1. Introduction

Although acetylcholine is one of major neurotransmitters in the peripheral autonomic nervous system as well as central nervous system (Collier, 1977; Fibiger, 1991; Calabresi et al., 2000), it has been difficult to measure endogenous acetylcholine in the in vivo state since acetylcholine released from nerve endings is rapidly degraded by tissue acetylcholinesterase (Taylor and Brown, 1998). Recently, microdialysis technique with improved measurement has made it possible to monitor low levels of acetylcholine in the in vivo central nervous system. In the peripheral autonomic nervous system, we have measured acetylcholine release from post-ganglionic parasympathetic nerve endings using microdialysis technique (Akiyama et al., 1994; Akiyama and Yamazaki, 2000, 2001; Kawada et al., 2001). Little information is, however, available on acetylcholine release from pre-ganglionic autonomic nerve endings in the in vivo state. The assessment of pre-ganglionic autonomic nerve activities is important for understanding the autonomic ganglionic transmission under physiological and pathophysiological conditions.

Adrenal medulla is one candidate suitable for investigating acetylcholine release from pre-ganglionic autonomic nerve endings (Holman et al., 1994). Compared to autonomic ganglia, adrenal gland is solid and suited to microdialysis probe implantation. Furthermore, microdialysis technique in the adrenal medulla provides a distinct advantage to monitor catecholamine release from adrenal medulla following acetylcholine release. Thus, we consider it possible to simultaneously assess pre- and post-ganglionic sympathetic nerve activities by monitoring acetylcholine and catecholamine release in the adrenal medulla.

In the present study, we applied the microdialysis technique to the adrenal medulla of anesthetized rats and tested the suitability of microdialysis technique to simultaneously

* Corresponding author. Tel.: +81-6-6833-5012x2380; fax: +81-6-6872-8092.
E-mail address: takiyama@ri.ncvc.go.jp (T. Akiyama).

0197-0186/$ – see front matter © 2003 Elsevier Ltd. All rights reserved.
doi:10.1016/j.neuint.2003.09.001

monitor acetylcholine and catecholamine release from adrenal medulla.

2. Materials and methods

2.1. Animal preparation

The investigation conforms with the *Guide for the Care and Use of Laboratory Animals* published by the US National Institutes of Health (NIH Publication No. 85-23, revised 1996). Adult male Wistar rats weighing 390–460 g were anesthetized with pentobarbital sodium (50–55 mg/kg i.p.). The rats were ventilated with a constant-volume respirator using room air mixed with oxygen. The left femoral artery and vein were cannulated for monitoring arterial blood pressure and administration of anesthetic, respectively. The level of anesthesia was maintained with a continuous intravenous infusion of pentobarbital sodium (15–25 mg/(kg h) i.v.). Electrocardiogram was monitored for recording heart rate. A thermostatic heating pad was used to keep the esophageal temperature within a range of 37–38 °C. With the animal in the lateral position, the left adrenal gland and left splanchnic nerve were exposed by a subcostal flank incision, and the left splanchnic nerve was transected. In protocols requiring nerve stimulation, shielded bipolar stainless steel electrodes were applied to the distal end of the nerve, which was then stimulated with a digital stimulator (SEN-7203, Nihon Kohden, Japan) with a rectangular pulse (10 V and 1 ms in duration).

2.2. Dialysis technique

The materials of the dialysis probe were the same as those used in our previous dialysis experiments (Akiyama et al., 2003). Briefly, each end of the dialysis fiber (0.31 mm o.d., and 0.20 mm i.d.; PAN-1200 50,000 mol. wt. cutoff, Asahi Chemical, Japan) was inserted into the polyethylene tube (25 cm length, 0.50 mm o.d., and 0.20 mm i.d.; SP-8) and glued. The length of the dialysis fiber exposed was 3 mm. At perfusion speed of 10 μl/min, in vitro recovery rates of acetylcholine, choline, norepinephrine, and epinephrine were (%): 3.08 ± 0.04, 2.93 ± 0.10, 2.09 ± 0.03, and 2.16 ± 0.03, respectively (number of dialysis probes: 3).

The dialysis probe was implanted in the medulla of the left adrenal gland and perfused with Ringer's solution containing the cholinesterase inhibitor, neostigmine (10 μM) at a speed of 10 μl/min using a microinjection pump (CMA/100, Carnegie Medicin, Sweden). Ringer's solution consisted of (in mM) 147.0 NaCl, 4.0 KCl, 2.25 $CaCl_2$. All pharmacological agents tested were locally administered by perfusion through the dialysis probe after being dissolved in Ringer's solution. One sampling period was 2 min (one sample volume = 20 μl). We started the protocols followed by a stabilization period of 3–4 h. Catecholamine release was evoked by 2 min-local administration of acetylcholine or 2 min-electrical stimulation of left splanchnic nerves. In protocols requiring repeated nerve stimulation, electrical stimulation was performed at 30 min-intervals. Taking the dead space volume into account, we continuously collected three dialysate samples per pharmacological or electrical stimulation: one before, one during, and one after stimulation. We subtracted the dialysate acetylcholine, norepinephrine, or epinephrine contents in control from those during stimulation, and expressed these values as indices of dialysate acetylcholine, norepinephrine or epinephrine response to stimulation.

Half of the dialysate sample was injected into high-performance liquid chromatography for the measurement of acetylcholine and choline (Akiyama et al., 1994), and the remaining half was injected into another high-performance liquid chromatography for the measurement of norepinephrine and epinephrine (Akiyama et al., 1991).

2.3. Experimental protocols

2.3.1. Protocol 1

We repeated stimulations of splanchnic nerves at 2 and 4 Hz twice and examined dialysate acetylcholine, choline and catecholamine responses to nerve stimulation and their reproducibility in five rats.

2.3.2. Protocol 2

To compare the estimated interstitial acetylcholine levels between administration of acetylcholine and nerve stimulation, we locally administered acetylcholine (10 μM) in five rats and stimulated splanchnic nerves at 2 Hz in five other rats. The concentration of exogenous acetylcholine was determined to obtain a similar dialysate catecholamine response to nerve stimulation at 2 Hz.

2.3.3. Protocol 3

We raised stepwise the frequency of nerve stimulation from 2 to 4, 10, 20 Hz and examined dialysate acetylcholine and catecholamine responses in five rats. In addition, to examine the input–output relationship in the adrenal medulla, we analyzed the relationship between dialysate acetylcholine and catecholamine responses of five rats.

2.3.4. Protocol 4

We examined the effects of cholinergic receptor antagonists on dialysate acetylcholine and catecholamine responses. Nerve stimulations at 2 and 4 Hz were performed before and after 30 min-local administration of cholinergic receptor antagonists. We tested the nicotinic receptor antagonist, hexamethonium bromide (1 mM) in five rats or the muscarinic receptor antagonist, atropine sulfate (10 μM) in five other rats.

2.4. Statistical methods

To examine the effect of nerve stimulation and pharmacological agents, we analyzed heart rate and mean

arterial pressure, and dialysate acetylcholine, choline, norepinephrine and epinephrine responses, using one- or two-way analysis of variance with repeated measures. When statistical significance was detected, the Newman–Keuls test was applied (Winer, 1971). Statistical significance was defined as $P < 0.05$. Values are presented as mean ± S.E.

3. Results

The experiments were carried in anesthetized rats and had been performed in the presence of neostigmine. Local administration of pharmacological agents did not influence heart rate or mean arterial pressure in any of the protocols. In protocol 3 ($n = 5$), nerve stimulation at 2 Hz decreased heart rate from 420 ± 8 to 397 ± 8 beats/min ($P < 0.05$) and increased mean arterial pressure from 125 ± 4 to 136 ± 3 mmHg ($P < 0.05$). Heart rate and mean arterial pressure recovered after cessation of stimulation. Nerve stimulation at 4, 10 and 20 Hz decreased heart rate to 396±9, 393±7 and 392 ± 9 beats/min, respectively, and increased mean arterial pressure to 134±3, 141±3, and 142±3 mmHg, respectively. In the other protocols, nerve stimulation at 2 or 4 Hz evoked the same responses of heart rate and mean arterial pressure.

3.1. Dialysate acetylcholine and catecholamine

3.1.1. Protocol 1

As shown in the *upper panel* of Fig. 1 ($n = 5$), acetylcholine was not detected in dialysate before nerve stimulation, but substantial acetylcholine was detected in dialysate by nerve stimulation. In contrast, choline, norepinephrine, and epinephrine were detected in dialysate before stimulation. Dialysate choline concentration did not change with repetitive nerve stimulation. Dialysate norepinephrine and epinephrine concentrations increased with nerve stimulation. Stimulation at the same frequency elicited almost identical responses on repetition.

3.1.2. Protocol 2

Using in vitro recovery rate of acetylcholine (3.08%), the estimated interstitial acetylcholine levels were 308 nM in acetylcholine infusion (10 μM, $n = 5$) and 276 ± 15 nM in nerve stimulation (2 Hz, $n = 5$; Fig. 1, *lower panel*). There was no statistical difference in the estimated interstitial acetylcholine levels and dialysate catecholamine responses between the two groups.

3.1.3. Protocol 3

When the frequency of nerve stimulation was increased from 2 to 20 Hz, dialysate acetylcholine, norepinephrine and epinephrine responses were enhanced ($n = 5$; Fig. 2, *upper panel*). We plotted the relationship between dialysate catecholamine response (ordinate) and dialysate acetylcholine response (abscissa) of five rats (Fig. 2, *lower panel*). Dialysate norepinephrine and epinephrine responses correlated with dialysate acetylcholine responses.

3.1.4. Protocol 4

At both 2 and 4 Hz of nerve stimulation, hexamethonium suppressed dialysate norepinephrine and epinephrine responses, but did not affect acetylcholine response ($n = 5$; Fig. 3, *upper panel*). Atropine suppressed epinephrine response at both 2 and 4 Hz of nerve stimulation, but did not affect norepinephrine and acetylcholine responses ($n = 5$; Fig. 3, *lower panel*).

4. Discussion

By now, simultaneous monitoring of adrenal acetylcholine and catecholamine release has been limited to only a few studies using perfused adrenal gland. Collier et al. (1984) measured endogenous acetylcholine and catecholamine effluxes from perfused cat adrenal gland. O'Farrell et al. (1997) preloaded bovine adrenal glands with [^{3}H]-choline and measured the subsequent efflux of [^{3}H]-labelled compound as an index of acetylcholine release and catecholamine efflux. In the present in vivo study, dialysate acetylcholine and catecholamine responses served as indices of acetylcholine release from splanchnic nerve endings and catecholamine release from adrenal medulla, respectively. This simultaneous monitoring implies quantitative measurement of pre- and post-ganglionic neurotransmitter release at the adrenal medulla.

4.1. Source of dialysate acetylcholine

The stimulation of splanchnic nerve induced acetylcholine release from pre-ganglionic nerve endings and increased dialysate acetylcholine concentration. It has been demonstrated that adrenal gland receives parasympathetic efferent and afferent innervation (Coupland et al., 1989; Niijima, 1992; Parker et al., 1993). Branches of parasympathetic efferent nerves conduct through celiac nerves, celiac ganglion and splanchnic nerves to adrenal nerves (Niijima, 1992). In the present study, we electrically stimulated the portion just distal to the sympathetic chain and proximal to the celiac ganglion. This portion does not contain branches of parasympathetic efferent nerves. After transection of splanchnic nerves, basal dialysate acetylcholine was less than the detection limit of high performance liquid chromatography (10 fmol), and substantial acetylcholine was detected in dialysate during the stimulation of this portion. Thus, most of the detected acetylcholine in dialysate derives from pre-ganglionic sympathetic nerve endings.

4.2. Interstitial choline levels in the adrenal medulla

Under physiological conditions, there is enough acetylcholinesterase activity in splanchnic nerve endings, chromaffin cells, and interstitial cells (Coupland, 1965; Palkama, 1967; Lewis and Shute, 1969; Somogyi et al., 1975). Released acetylcholine is degraded to choline and acetate by

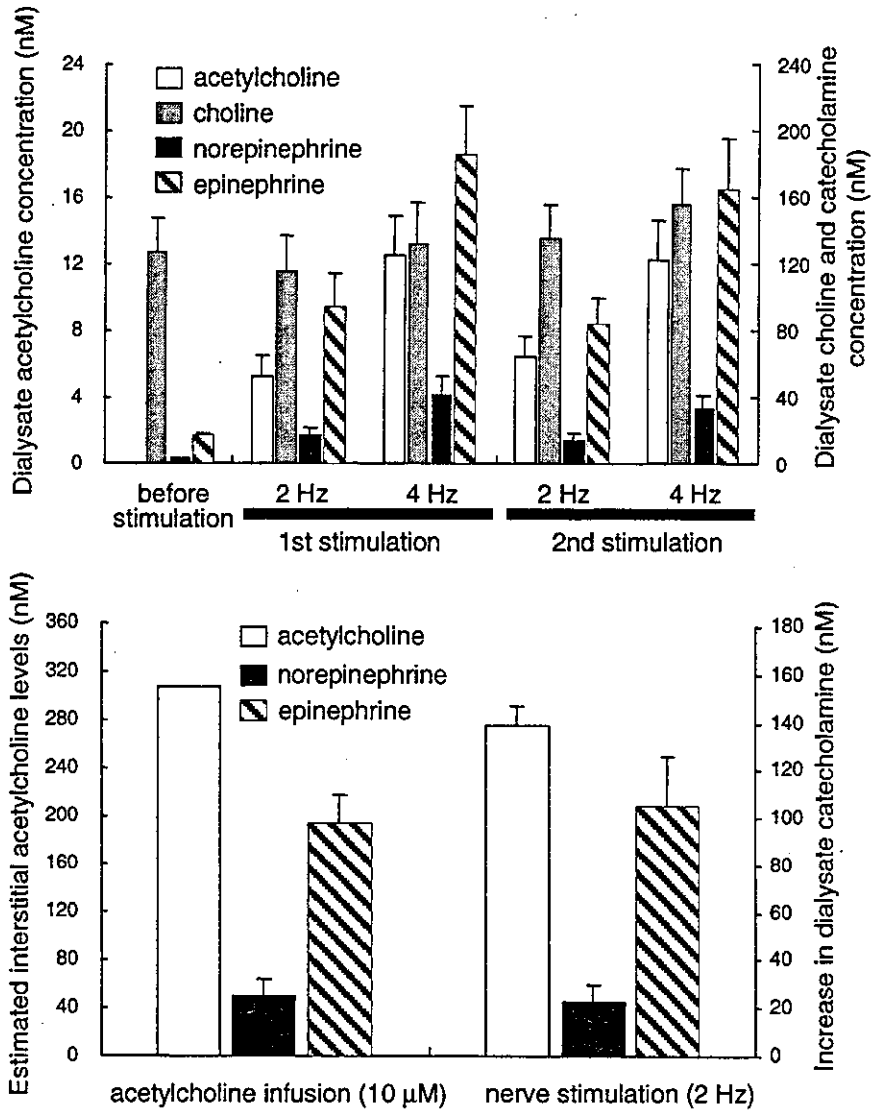

Fig. 1. (*Upper panel*) Acetylcholine was not detected in dialysate before nerve stimulation, but substantial acetylcholine was detected in dialysate by nerve stimulation (5 ± 1 nM at 2 Hz and 12 ± 2 nM at 4 Hz). Dialysate choline concentration did not change with nerve stimulation. Dialysate norepinephrine and epinephrine concentrations increased with nerve stimulation (17 ± 5 and 94 ± 20 nM at 2 Hz, respectively, and 41 ± 12 and 185 ± 29 nM at 4 Hz, respectively). Stimulation at the same frequency elicited almost identical responses on repetition, $n = 5$. Values are mean ± S.E. (*Lower panel*) There was no statistical difference in the estimated interstitial acetylcholine levels and dialysate catecholamine responses between acetylcholine infusion (10 μM, $n = 5$) and nerve stimulation (2 Hz, $n = 5$). Values are mean ± S.E.

acetylcholinesterase. Interstitial choline is carried into the nerve endings through neuronal transporters and used as a precursor for synthesis of acetylcholine (Taylor and Brown, 1998). In in vitro perfused experiments, continuous administration of choline sustains the synthesis and release of acetylcholine from nerve endings. In the present study, the concentration of dialysate choline was more than 10 times that of dialysate acetylcholine during nerve stimulation, and repetitive acetylcholine release did not induce a decrease in dialysate choline concentration. Moreover, nerve stimulation elicited almost identical responses of dialysate acetylcholine on repetition. These results indicate that repetitive acetylcholine release did not decrease interstitial choline levels and did not affect release of acetylcholine. Thus, under in vivo conditions, adrenal interstitial choline levels may be sufficiently high to sustain acetylcholine synthesis in the pre-ganglionic nerve endings.

4.3. Catecholamine release induced by endogenous and exogenous acetylcholine

Either exogenous or endogenous acetylcholine evokes catecholamine release by activating cholinergic receptors on the surface of chromaffin cells (Douglas, 1975). The interstitial acetylcholine levels serves as an index of input into chromaffin cells. We examined whether the estimated interstitial acetylcholine levels were identical between exogenous acetylcholine and nerve stimulation when

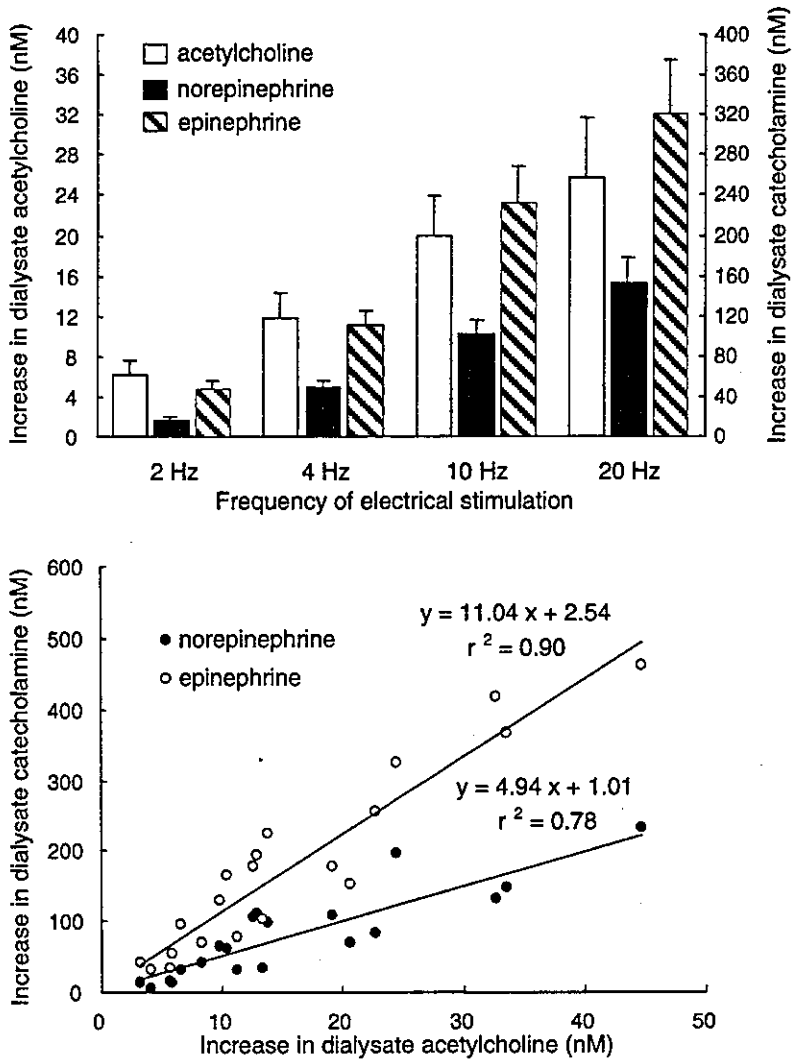

Fig. 2. (*Upper panel*) Dialysate acetylcholine response was enhanced from 6 ± 1 to 26 ± 6 nM when the frequency of nerve stimulation was increased from 2 to 20 Hz. Similarly, dialysate norepinephrine and epinephrine responses were enhanced from 16 ± 4 to 152 ± 26 nM and 48 ± 9 to 321 ± 54 nM, respectively, $n = 5$. Values are mean ± S.E. (*Lower panel*) The relationship between dialysate catecholamine response (*ordinate*) and dialysate acetylcholine response (*abscissa*) of five rats. Dialysate norepinephrine and epinephrine responses correlated with dialysate acetylcholine responses. These relations were expressed by regression equations with correlation coefficients of $y = 4.94x + 1.01$, $r^2 = 0.78$, and $y = 11.04x + 2.54$, $r^2 = 0.90$, respectively.

dialysate catecholamine responses were equal. Actually the estimated interstitial acetylcholine levels during nerve stimulation (2 Hz) were identical with those during acetylcholine infusion (10 μM). These data indicate that inputs into chromaffin cells were almost identical between the two stimulations. It could be inferred from this finding that dialysate acetylcholine concentration reflects acetylcholine levels at the surface of chromaffin cells and serves as an index of cholinergic transmission in the adrenal medulla.

4.4. Relationship of acetylcholine and catecholamine release

Dialysate norepinephrine and epinephrine responses were correlated with the frequency of splanchnic nerve stimulation. This norepinephrine and epinephrine release occurred as a consequence of acetylcholine release by splanchnic nerve stimulation. We found a linear relation between dialysate acetylcholine response and dialysate catecholamine responses. This indicates that the input–output relationship in the adrenal medulla is linear over the range of frequency from 2 to 20 Hz. Dialysate acetylcholine response of 1 nM evoked dialysate norepinephrine response of about 5 nM and dialysate epinephrine response of about 11 nM. This relation between dialysate acetylcholine and catecholamine responses could provide quantitative information about the input–output relationship in the adrenal medulla.

4.5. Effects of cholinergic receptor antagonists

It has been suggested that acetylcholine release from pre-ganglionic nerve endings is modulated by pre-synaptic

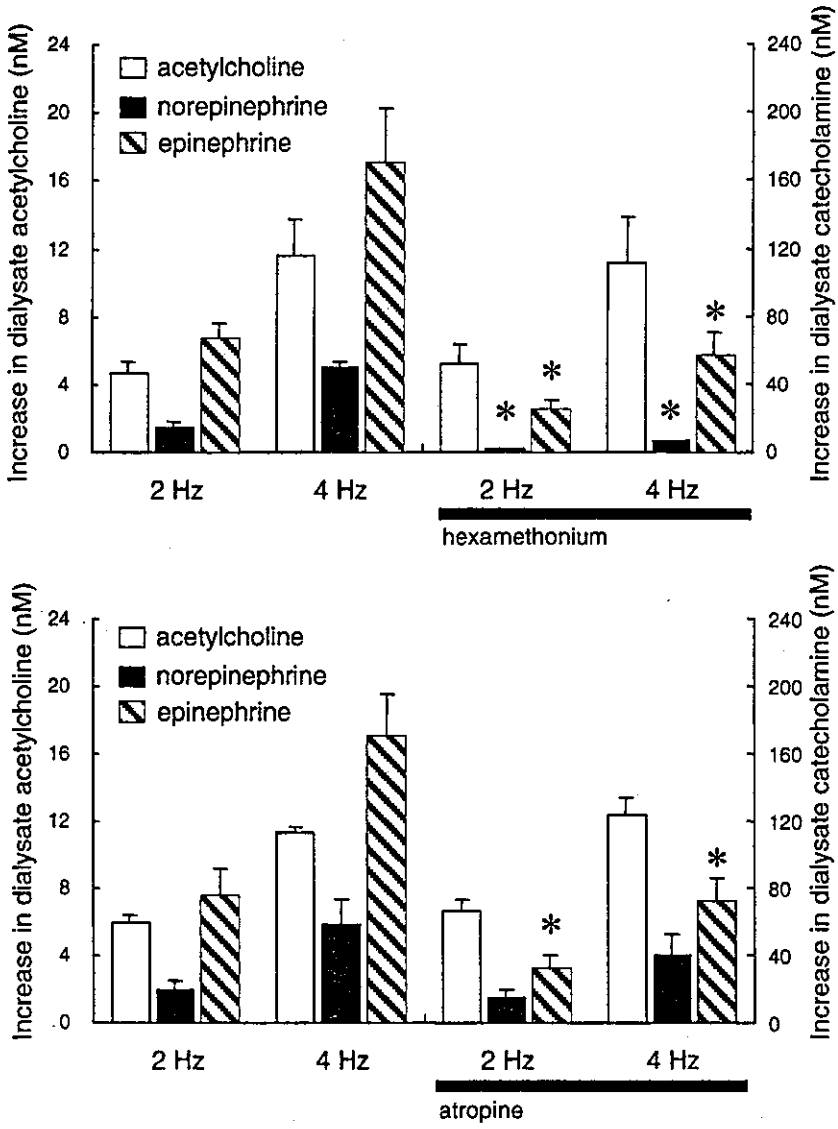

Fig. 3. (*Upper panel*) At both 2 and 4 Hz of nerve stimulation, hexamethonium suppressed dialysate norepinephrine and epinephrine responses, but did not affect acetylcholine response, $n = 5$. Values are mean ± S.E. $^*P < 0.05$ vs. concurrent dialysate norepinephrine or epinephrine response before administration of hexamethonium. (*Lower panel*) At both 2 and 4 Hz of nerve stimulation, atropine suppressed epinephrine response, but did not affect norepinephrine and acetylcholine responses, $n = 5$. Values are mean ± S.E. $^*P < 0.05$ vs. concurrent dialysate norepinephrine or epinephrine response before administration of atropine.

cholinergic autoreceptors (Dujic et al., 1990; Myers and Undem, 1996; Barbara et al., 1998). Neostigmine might induce the activation of pre-synaptic cholinergic receptors by increasing the acetylcholine levels in synaptic regions (Brehm et al., 1992) and suppress acetylcholine release by activating pre-synaptic autoreceptors. In the present study, neither hexamethonium nor atropine affected dialysate acetylcholine response to nerve stimulation at either 2 or 4 Hz. Thus, autoinhibition of acetylcholine release can be considered insignificant in our experimental condition, and dialysate acetylcholine response reflects pre-ganglionic nerve activities. In contrast, hexamethonium suppressed norepinephrine and epinephrine releases by nerve stimulation whereas atropine suppressed only epinephrine release. The muscarinic agonist, muscarine or pilocarpine preferentially enhanced epinephrine release (Douglas and Poisner, 1965; Wakade and Wakade, 1983). These results suggest that both nicotinic and muscarinic receptors exist on the surface of epinephrine-storing cells, while, on the surface of norepinephrine-storing cells, nicotinic receptors are primarily present.

4.6. Methodological limitations

We locally administered neostigmine to adrenal medulla through dialysis probe. Cholinesterase inhibitor was necessary to detect acetylcholine even during splanchnic nerve stimulation because released acetylcholine is rapidly

degraded by acetylcholinesterase before reaching the dialysis fiber. In the same preparation, local administration of neostigmine enhanced the dialysate catecholamine response to nerve stimulation by about three-fold, but did not influence the responses of heart rate and mean arterial pressure (Akiyama et al., 2003). Total catecholamine release from adrenal gland might not change by the local administration of neostigmine. In the present study, dialysate catecholamine response was correlated with the frequency of splanchnic nerve stimulation. Thus, in the presence of neostigmine, absolute value of dialysate catecholamine response is exaggerated, but could reflect relative changes in catecholamine release from adrenal gland.

Acknowledgements

This study was supported by the Program for Promotion of Fundamental Studies in Health Science of the Organization for Pharmaceutical Safety and Research (of Japan); by a Health Sciences Research Grant for Advanced Medical Technology from the Ministry of Health and Welfare of Japan; by a Ground-Based Research Grand for the Space Utilization promoted by NASDA (National Space Development Agency of Japan) and Japan Space Forum; by Grants-in-Aid for scientific research from the Ministry of Education, Science.

References

Akiyama, T., Yamazaki, T., 2000. Adrenergic inhibition of endogenous acetylcholine release on post-ganglionic cardiac vagal nerve terminals. Cardiovasc. Res. 46, 531–538.

Akiyama, T., Yamazaki, T., 2001. Effects of right and left vagal stimulation on left ventricular acetylcholine levels in the cat. Acta Physiol. Scand. 172, 11–16.

Akiyama, T., Yamazaki, T., Ninomiya, I., 1991. In vivo monitoring of myocardial interstitial norepinephrine by dialysis technique. Am. J. Physiol. 261, H1643–H1647.

Akiyama, T., Yamazaki, T., Ninomiya, I., 1994. In vivo detection of endogenous acetylcholine release in cat ventricles. Am. J. Physiol. 266, H854–H860.

Akiyama, T., Yamazaki, T., Mori, H., Sunagawa, K., 2003. Inhibition of cholinesterase elicits muscarinic receptor-mediated synaptic transmission in the rat adrenal medulla. Auton. Neurosci.: Basic Clin. 107, 65–73.

Barbara, J.G., Lemos, V.S., Takeda, K., 1998. Pre- and post-synaptic muscarinic receptors in thin slices of rat adrenal gland. Eur. J. Neurosci. 10, 3535–3545.

Brehm, G., Lindmar, R., Löffelholz, K., 1992. Inhibitory and excitatory muscarinic receptors modulating the release of acetylcholine from the post-ganglionic parasympathetic neuron of the chicken heart. Naunyn-Schmiedeberg's Arch. Pharmacol. 346, 375–382.

Calabresi, P., Centonze, D., Gubellini, P., Pisani, A., Bernardi, G., 2000. Acetylcholine-mediated modulation of striatal function. Trends Neurosci. 23, 120–126.

Collier, B., 1977. Biochemistry and physiology of cholinergic transmission. In: Handbook of Physiology. The Nervous System. Cellular Biology of Neurons, Section 1, Part 1. Amercian Physiological Soceity, Bethesda, MD, Chapter 13, pp. 463–492.

Collier, B., Johnson, G., Kirpekar, S.M., Prat, J., 1984. The release of acetylcholine and of catecholamine from the cat's adrenal gland. Neuroscience 13, 957–964.

Coupland, R.E., 1965. The Natural History of the Chromaffin Cell. Longmans, London.

Coupland, R.E., Parker, T.L., Kesse, W.K., Mohamed, A.A., 1989. The innervation of the adrenal gland. Part III. Vagal innervation. J. Anat. 163, 173–181.

Douglas, W.W., 1975. Secretomotor control of adrenal medullary secretion: synaptic, membrane, and ionic events in stimulus–secretion coupling. In: Handbook of Physiology. Endocrinology. Adrenal Gland, Section 7, vol. VI. Amercian Physiological Soceity, Bethesda, MD, Chapter 26, pp. 367–388.

Douglas, W.W., Poisner, A.M., 1965. Preferential release of adrenaline from the adrenal medulla by muscarine and pilocarpine. Nature 208, 1102–1103.

Dujic, Z., Roerig, D.L., Schedewie, H.K., Kampine, J.P., Bosnjak, Z.J., 1990. Presynaptic modulation of ganglionic ACh release by muscarinic and nicotinic receptors. Am. J. Physiol. 259, R288–R293.

Fibiger, H.C., 1991. Cholinergic mechanisms in learning, memory and dementia: a review of recent evidence. Trends Neurosci. 14, 220–223.

Holman, M.E., Coleman, H.A., Tonta, M.A., Parkington, H.C., 1994. Synaptic transmission from splanchnic nerves to the adrenal medulla of guinea-pigs. J. Physiol. 478, 115–124.

Kawada, T., Yamazaki, T., Akiyama, T., Shishido, T., Inagaki, M., Uemura, K., Miyamoto, T., Sugimachi, M., Takaki, H., Sunagawa, K., 2001. In vivo assessment of acetylcholine-releasing function at cardiac vagal nerve terminals. Am. J. Physiol. 281, H139–H145.

Lewis, P.R., Shute, C.C., 1969. An electron-microscopic study of cholinesterase distribution in the rat adrenal medulla. J. Microsc. 89, 181–193.

Myers, A.C., Undem, B.J., 1996. Muscarinic receptor regulation of synaptic transmission in airway parasympathetic ganglia. Am. J. Physiol. 270, L630–L636.

Niijima, A., 1992. Electrophysiological study on the vagal innervation of the adrenal gland in the rat. J. Auton. Nerv. Syst. 41, 87–92.

O'Farrell, M., Ziogas, J., Marley, P.D., 1997. Effects of N- and L-type calcium channel antagonists and (±)-Bay K8644 on nerve-induced catecholamine secretion from bovine perfused adrenal glands. Br. J. Pharmacol. 121, 381–388.

Palkama, A., 1967. Demonstration of adrenomedullary catecholamines and cholinesterases at electron microscopic level in the same tissue section. Ann. Med. Exp. Biol. Fenn. 45, 295–306.

Parker, T.L., Kesse, W.K., Mohamed, A.A., Afework, M., 1993. The innervation of the mammalian adrenal gland. J. Anatom. 183, 265–276.

Somogyi, P., Chubb, I.W., Smith, A.D., 1975. A possible structural basis for the extracellular release of acetylcholinesterase. In: Proceedings of the Royal Society of London, Series B. Biol. Sci. 191, 271–283.

Taylor, P., Brown, J.H., 1998. Acetylcholine. In: Siegel, G., Agranoff, B., Albers, R., Fisher, S., Uhler, M. (Eds.), Basic Neurochemistry, sixth ed. Lippincott–Raven, Philadelphia–New York, pp. 213–242.

Wakade, A.R., Wakade, T.D., 1983. Contribution of nicotinic and muscarinic receptors in the secretion of catecholamines evoked by endogenous and exogenous acetylcholine. Neuroscience 10, 973–978.

Winer, B.J., 1971. Statistical Principles in Experimental Design, Second ed. McGraw-Hill, New York.

Am J Physiol Regul Integr Comp Physiol 287: R161–R166, 2004.
First published March 18, 2004; 10.1152/ajpregu.00609.2003.

Effects of Ca^{2+} channel antagonists on acetylcholine and catecholamine releases in the in vivo rat adrenal medulla

Tsuyoshi Akiyama,[1] Toji Yamazaki,[1] Hidezo Mori,[1] and Kenji Sunagawa[2]

[1]*Department of Cardiac Physiology and* [2]*Department of Cardiovascular Dynamics, National Cardiovascular Center Research Institute, Suita, Osaka 565–8565, Japan*

Submitted 20 October 2003; accepted in final form 13 March 2004

Akiyama, Tsuyoshi, Toji Yamazaki, Hidezo Mori, and Kenji Sunagawa. Effects of Ca^{2+} channel antagonists on acetylcholine and catecholamine releases in the in vivo rat adrenal medulla. *Am J Physiol Regul Integr Comp Physiol* 287: R161–R166, 2004. First published March 18, 2004; 10.1152/ajpregu.00609.2003.—To elucidate the types of voltage-dependent Ca^{2+} channels controlling ACh and catecholamine releases in the in vivo adrenal medulla, we implanted microdialysis probes in the left adrenal medulla of anesthetized rats and investigated the effects of Ca^{2+} channel antagonists on ACh, norepinephrine, and epinephrine releases induced by nerve stimulation. The dialysis probes were perfused with Ringer solution containing a cholinesterase inhibitor, neostigmine. The left splanchnic nerves were electrically stimulated at 2 and 4 Hz before and after intravenous administration of Ca^{2+} channel antagonists. ω-Conotoxin GVIA (an N-type Ca^{2+} channel antagonist, 10 μg/kg) inhibited ACh release at 2 and 4 Hz by ~40%, norepinephrine release at 4 Hz by ~50%, and epinephrine release at 2 and 4 Hz by ~45%. A fivefold higher dose of ω-conotoxin GVIA (50 μg/kg) did not further inhibit these releases. ω-Conotoxin MVIIC (a P/Q-type Ca^{2+} channel antagonist, 50 μg/kg) inhibited ACh and epinephrine releases at 4 Hz by ~30%. Combined ω-conotoxin GVIA (50 μg/kg) and MVIIC (250 μg/kg) inhibited ACh release at 2 and 4 Hz by ~70% and norepinephrine and epinephrine releases at 2 and 4 Hz by ~80%. Nifedipine (an L-type Ca^{2+} channel antagonist, 300 and 900 μg/kg) did not change ACh release at 2 and 4 Hz; however, nifedipine (300 μg/kg) inhibited epinephrine release at 4 Hz by 20%, and nifedipine (900 μg/kg) inhibited norepinephrine and epinephrine releases at 4 Hz by 30%. In conclusion, both N- and P/Q-type Ca^{2+} channels control ACh release on preganglionic splanchnic nerve endings while L-type Ca^{2+} channels do not. L-type Ca^{2+} channels are involved in norepinephrine and epinephrine releases on chromaffin cells.

anesthetized rats; microdialysis; norepinephrine; epinephrine; preganglionic autonomic nerve endings

Ca^{2+} influx through the voltage-dependent Ca^{2+} channels induces the release of transmitters from neuronal or secretory cells by initiating exocytosis from vesicles. Voltage-dependent Ca^{2+} channels have been classified into L-, N-, P-, Q-, R-, and T-types (12, 25, 30). To better understand the mechanism controlling the release of transmitters, it is important to determine the type of Ca^{2+} channels involved in the release of the transmitters on neuronal or secretory cells.

In the in vivo adrenal medulla, catecholamine release is controlled by central sympathetic neurons through preganglionic splanchnic nerves. Splanchnic nerve endings make synaptic-like contacts with chromaffin cells (9). ACh released from splanchnic nerve endings consequently evokes catecholamine release from chromaffin cells by activation of cholinergic receptors. Thus, in vivo catecholamine release requires Ca^{2+} influx through the voltage-dependent Ca^{2+} channels at two different sites in the adrenal medulla: splanchnic nerve endings and chromaffin cells. Numerous studies have investigated the nature of Ca^{2+} channels controlling transmitter release from postganglionic autonomic nerve endings (8, 11, 32, 33, 36, 37). Little information is, however, available on the type of Ca^{2+} channels controlling the ACh release from preganglionic autonomic nerve endings including splanchnic nerve endings. Moreover, although the types of Ca^{2+} channels controlling catecholamine release have been investigated using isolated chromaffin cells in various species (5, 6, 13, 16, 21, 23, 24), it remains unknown whether endogenous ACh induces Ca^{2+} influx through the same types of Ca^{2+} channels on chromaffin cells.

We have recently developed a dialysis technique to simultaneously monitor ACh and catecholamine releases in the in vivo adrenal medulla (2). This method makes it possible to characterize Ca^{2+} channels controlling ACh release from splanchnic nerve endings and catecholamine release from adrenal medulla in the in vivo state. In the present study, we applied the microdialysis technique to the adrenal medulla of anesthetized rats and investigated the effects of Ca^{2+} channel antagonists on dialysate ACh and catecholamine responses induced by the electrical stimulation of splanchnic nerves.

MATERIALS AND METHODS

Animal preparation. The investigation conforms with the *Guide for the Care and Use of Laboratory Animals* published by the National Institutes of Health (NIH Publication No. 85–23, revised 1996). Adult male Wistar rats weighing 380–450 g were anesthetized with pentobarbital sodium (50–55 mg/kg ip). A cervical midline incision was made to expose the trachea, which was then cannulated. The rats were ventilated with a constant-volume respirator using room air mixed with oxygen. The left femoral artery and vein were cannulated for monitoring arterial blood pressure and administration of anesthetic, respectively. The level of anesthesia was maintained with a continuous intravenous infusion of pentobarbital sodium (15–25 $mg \cdot kg^{-1} \cdot h^{-1}$ iv). Electrocardiogram was monitored for recording heart rate. A thermostatic heating pad was used to keep the esophageal temperature within a range of 37–38°C. With the animal in the lateral position, the left adrenal gland and left splanchnic nerve were exposed by a subcostal flank incision, and the left splanchnic nerve was transected. Shielded bipolar stainless steel electrodes were applied to the distal end of the nerve, which was then stimulated with a digital stimulator (SEN-7203, Nihon Kohden) with a rectangular pulse (10 V and 1 ms in duration).

Address for reprint requests and other correspondence: T. Akiyama, Dept. of Cardiac Physiology, National Cardiovascular Center Research Institute, 5-7-1 Fujishiro-dai, Suita, Osaka, 565–8565 Japan (E-mail: takiyama@ri.ncvc.go.jp).

The costs of publication of this article were defrayed in part by the payment of page charges. The article must therefore be hereby marked "*advertisement*" in accordance with 18 U.S.C. Section 1734 solely to indicate this fact.

Dialysis technique. The materials of the dialysis probe were the same as those used in our previous dialysis experiments (1, 2). Briefly, each end of the dialysis fiber (0.31 mm OD, and 0.20 mm ID; PAN-1200 50,000 mol wt cutoff, Asahi Chemical) was inserted into the polyethylene tube (25-cm length, 0.5 mm OD, and 0.2 mm ID; SP-8) and glued. The length of the dialysis fiber exposed was 3 mm.

The left adrenal gland was gently lifted, and the dialysis probe was implanted in the medulla of the left adrenal gland along the long axis by using a fine guiding needle. The dialysis probe was perfused with Ringer solution containing a cholinesterase inhibitor, neostigmine (10 μM), at a speed of 10 μl/min using a microinjection pump (CMA/100, Carnegie Medicin). Ringer solution with no buffer consisted of (in mM) 147.0 NaCl, 4.0 KCl, and 2.25 $CaCl_2$. One sampling period was 2 min (1 sample volume = 20 μl). We started the protocols followed by a stabilization period of 3–4 h and sampled dialysate taking the dead space volume into account.

Dialysate ACh, norepinephrine (NE), and epinephrine (Epi) concentrations were measured as indexes of ACh and catecholamine releases in the adrenal medulla. Half of the dialysate sample was used for the measurement of ACh, and the remaining half for the measurement of NE and Epi. ACh and catecholamine assays were separately conducted using each high-performance liquid chromatography with electrochemical detection as previously described (3, 4).

Experimental design. The experiment was performed based on the previous experiment showing that dialysate ACh and catecholamine responses were reproducible on repetition of stimulation (2). The left splanchnic nerves were electrically stimulated for 2 min at 30-min intervals. Three dialysate samples were continuously collected per electrical stimulation: one before, one during, and one after stimulation. Stimulations at two different frequencies (2 and 4 Hz) were performed before and after intravenous administration of Ca^{2+} channel antagonists.

We tested three types of Ca^{2+} channel antagonists (25): the N-type Ca^{2+} channel antagonist ω-conotoxin GVIA, the P/Q-type Ca^{2+} channel antagonist ω-conotoxin MVIIC, and the L-type Ca^{2+} channel antagonist nifedipine. We determined the first doses of Ca^{2+} channel antagonists based on the dose used in the earlier experiments (7, 14, 26, 29, 37) and tested ω-conotoxin GVIA (10 μg/kg) in six rats, ω-conotoxin MVIIC (50 μg/kg) in six rats, and nifedipine (300 μg/kg) in six rats. Second, we tested a fivefold higher dose of ω-conotoxin GVIA (50 μg/kg) in six rats, a combination of fivefold higher doses of ω-conotoxin GVIA (50 μg/kg) and MVIIC (250 μg/kg) in six rats, and a threefold higher dose of nifedipine (900 μg/kg) in six rats. We did not test a higher dose of ω-conotoxin MVIIC singly because a high dose of ω-conotoxin MVIIC loses its selectivity for P/Q-type and inhibits N-type Ca^{2+} channels (18).

Nifedipine was administered twice before 2- and 4-Hz stimulation, but ω-conotoxin GVIA and MVIIC were administered once before 2-Hz stimulation because the ω-conotoxin family has long-lasting blocking actions (8, 18, 36). We assessed the responses to nerve stimulation 30, 20, and 10 min after administration of ω-conotoxin GVIA, ω-conotoxin MVIIC, and nifedipine, respectively, when heart rate and arterial pressure had already been stabilized.

At the end of the experiment the rats were killed with pentobarbital sodium, and the implant sites were examined. The dialysis probes were confirmed to have been implanted in the adrenal medulla, and no bleeding or necrosis was found macroscopically.

Drugs. Drugs were mixed fresh for each experiment. Neostigmine methylsulfate (Shionogi), ω-conotoxin GVIA (Peptide Institute), and ω-conotoxin MVIIC (Peptide Institute) were dissolved and diluted in Ringer solution. Nifedipine (Sigma Chemical) was dissolved in ethanol and diluted in Ringer solution.

Statistical methods. To examine the effects of nerve stimulation and Ca^{2+} channel antagonists, we analyzed heart rate and mean arterial pressure and dialysate ACh, NE, and Epi responses by using one-way ANOVA with repeated measures. When statistical significance was detected, the Newman-Keuls test was applied (35). Statistical significance was defined as $P < 0.05$. Values are presented as means ± SE.

RESULTS

Effects of Ca^{2+} channel antagonists on heart rate and mean arterial pressure. ω-Conotoxin GVIA (10 μg/kg) decreased heart rate from 418 ± 9 to 328 ± 13 beats/min ($P < 0.05$) and mean arterial pressure from 115 ± 2 to 74 ± 2 mmHg ($P < 0.05$). ω-Conotoxin GVIA (50 μg/kg) did not further decrease heart rate and mean arterial pressure. ω-Conotoxin MVIIC decreased heart rate from 408 ± 3 to 390 ± 5 beats/min ($P < 0.05$) but did not change mean arterial pressure. Combined ω-conotoxin GVIA and MVIIC decreased heart rate from 415 ± 10 to 327 ± 4 beats/min ($P < 0.05$) and mean arterial pressure from 124 ± 2 to 57 ± 2 mmHg ($P < 0.05$). Nifedipine (300 μg/kg) decreased mean arterial pressure from 113 ± 4 to 86 ± 4 mmHg ($P < 0.05$) but did not change heart rate. Nifedipine (900 μg/kg) decreased mean arterial pressure from 124 ± 3 to 73 ± 2 mmHg ($P < 0.05$).

Effects of Ca^{2+} channel antagonists on ACh and catecholamine releases. ACh could not be detected in dialysate before or after stimulation. Thus we expressed dialysate ACh concentration during stimulation as an index of ACh release induced by stimulation. In contrast, substantial amounts of NE and Epi were observed in dialysate before stimulation. Intravenous administration of Ca^{2+} channel antagonists did not affect these basal NE and Epi releases (Table 1). Dialysate NE and Epi concentrations increased by nerve stimulation and rapidly declined after the stimulation. Thus we subtracted the dialysate NE and Epi contents before stimulation from those during stimulation and expressed these values as indexes of NE and Epi releases induced by stimulation.

Effects of ω-conotoxin GVIA. ω-Conotoxin GVIA (10 μg/kg) significantly inhibited ACh release at 2 Hz from 6.2 ± 0.9 to 3.6 ± 0.5 nM, ACh release at 4 Hz from 12.2 ± 1.7 to 7.9 ± 1.2 nM, NE release at 4 Hz from 34 ± 6 to 17 ± 3 nM, Epi release at 2 Hz from 81 ± 13 to 42 ± 3 nM, and Epi release at 4 Hz from 180 ± 21 to 94 ± 7 nM. However, inhibition of NE release at 2 Hz was not statistically significant (Fig. 1*A*). A fivefold higher dose of ω-conotoxin GVIA (50 μg/kg) did not

Table 1. *Basal dialysate NE and Epi concentrations before and after administration of Ca^{2+} channel antagonists*

	NE, nM	Epi, nM
ω-Conotoxin GVIA (10 and 50 μg/kg) (n = 12)		
Before administration	4.9±0.9	20.6±2.9
After administration	3.8±0.6	21.0±2.6
ω-Conotoxin MVIIC (50 μg/kg) (n = 6)		
Before administration	4.1±1.0	20.2±2.6
After administration	4.6±0.9	24.0±3.5
ω-Conotoxin GVIA (50 μg/kg) + MVIIC (250 μg/kg) (n = 6)		
Before administration	4.4±1.3	17.5±3.8
After administration	3.1±0.7	20.8±4.4
Nifedipine (100 and 300 μg/kg) (n = 12)		
Before administration	4.0±0.6	17.4±2.2
After administration	3.3±0.9	17.7±2.9

Values are means ± SE; *n*, no. of rats. NE, norepinephrine; Epi, epinephrine.

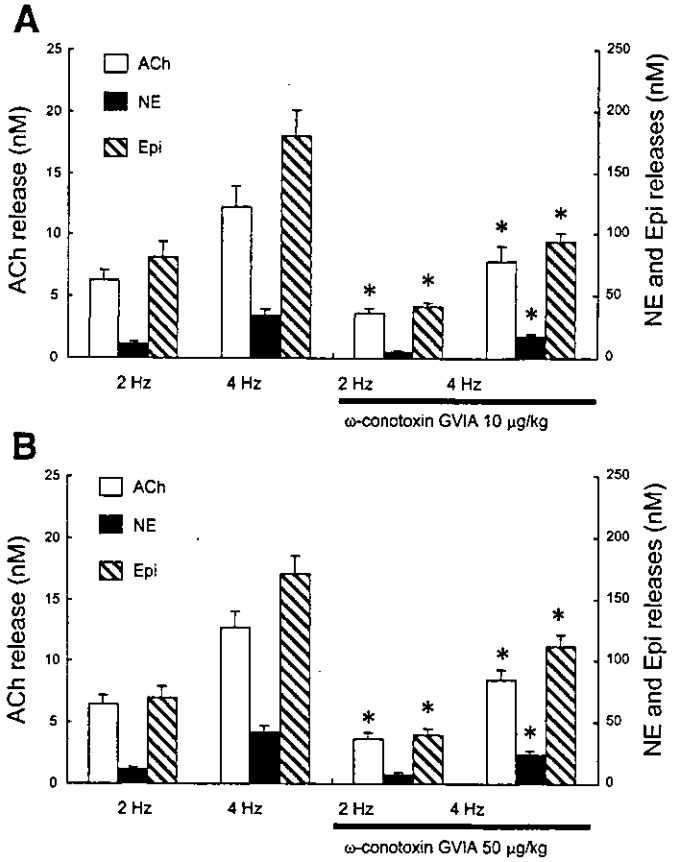

Fig. 1. Effects of ω-conotoxin GVIA on ACh, norepinephrine (NE), and epinephrine (Epi) releases. ω-Conotoxin GVIA (10 μg/kg) inhibited ACh release at 2 and 4 Hz, NE release at 4 Hz, and Epi release at 2 and 4 Hz (*A*). A 5-fold higher dose of ω-conotoxin GVIA (50 μg/kg) did not further inhibit these releases (*B*). Values are means ± SE from 6 rats. $*P < 0.05$ vs. ACh, NE, or Epi release at same frequency before administration.

further inhibit release. ω-Conotoxin GVIA (50 μg/kg) significantly inhibited ACh release at 2 Hz from 6.5 ± 0.7 to 3.7 ± 0.5 nM, ACh release at 4 Hz from 12.6 ± 1.4 to 8.5 ± 0.8 nM, NE release at 4 Hz from 41 ± 6 to 24 ± 4 nM, Epi release at 2 Hz from 70 ± 10 to 40 ± 6 nM, and Epi release at 4 Hz from 170 ± 15 to 112 ± 10 nM (Fig. 1*B*).

Effects of ω-conotoxin MVIIC. ω-Conotoxin MVIIC (50 μg/kg) significantly inhibited ACh release at 4 Hz from 11.7 ± 2.5 to 8.5 ± 2.1 nM and Epi release at 4 Hz from 170 ± 38 to 129 ± 35 nM. Inhibitions of ACh and Epi releases at 2 Hz and NE release at either frequency were not statistically significant (Fig. 2).

Effects of combined ω-conotoxin GVIA and MVIIC. Combined ω-conotoxin GVIA (50 μg/kg) and MVIIC (250 μg/kg) significantly inhibited ACh release at 2 Hz from 6.7 ± 0.6 to 1.9 ± 0.3 nM, ACh release at 4 Hz from 12.1 ± 1.3 to 3.8 ± 0.6 nM, NE release at 2 Hz from 11.1 ± 1.1 to 1.2 ± 0.3 nM, NE release at 4 Hz from 36 ± 5 to 8 ± 2 nM, Epi release at 2 Hz from 88 ± 9 to 13 ± 3 nM, and Epi release at 4 Hz from 187 ± 20 to 49 ± 9 nM (Fig. 3).

Effects of nifedipine. Nifedipine (300 μg/kg) did not change ACh release at either frequency but significantly inhibited Epi release at 4 Hz from 172 ± 31 to 135 ± 23 nM. Inhibitions of Epi release at 2 Hz and NE release at either frequency were not statistically significant (Fig. 4*A*). A threefold higher dose of

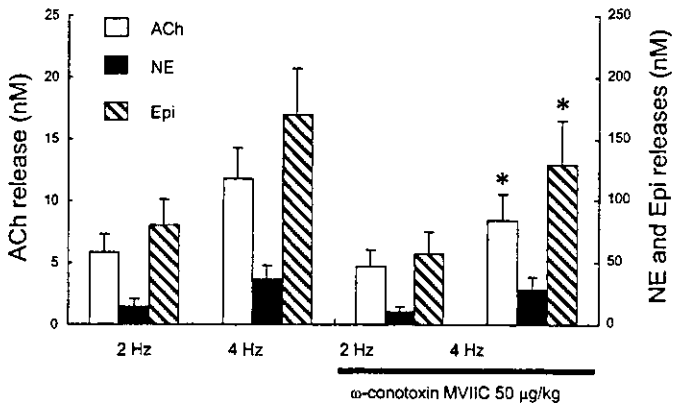

Fig. 2. Effects of ω-conotoxin MVIIC on ACh, NE, and Epi releases. ω-Conotoxin MVIIC (50 μg/kg) inhibited ACh and Epi releases at 4 Hz. Values are means ± SE from 6 rats. $*P < 0.05$ vs. ACh, NE, or Epi release at same frequency before administration.

nifedipine (900 μg/kg) did not change ACh release but significantly inhibited Epi release at 4 Hz from 188 ± 24 to 128 ± 15 nM and NE release at 4 Hz from 33 ± 5 to 24 ± 4 nM. Inhibitions of NE and Epi releases at 2 Hz were not statistically significant (Fig. 4*B*).

DISCUSSION

Effects of Ca^{2+} channel antagonists on ACh release from splanchnic nerve endings. In the present study, ω-conotoxin GVIA (10 μg/kg) inhibited ACh release at both 2 and 4 Hz by approximately 35–40%. A fivefold higher dose of ω-conotoxin GVIA (50 μg/kg) did not further inhibit ACh release. ω-Conotoxin MVIIC (50 μg/kg) inhibited ACh release at 4 Hz by ~30%. Combined ω-conotoxin GVIA (50 μg/kg) and MVIIC (250 μg/kg) inhibited ACh release at both 2 and 4 Hz by ~70%. N- and P/Q-type Ca^{2+} channels could be present on the splanchnic nerve endings and be involved in ACh release. P/Q-type Ca^{2+} channels may play a role in ACh release at a high frequency of stimulation. ACh release response was resistant to nifedipine (300 and 900 μg/kg) at both 2 and 4 Hz. L-type Ca^{2+} channels could not be present on splanchnic nerve

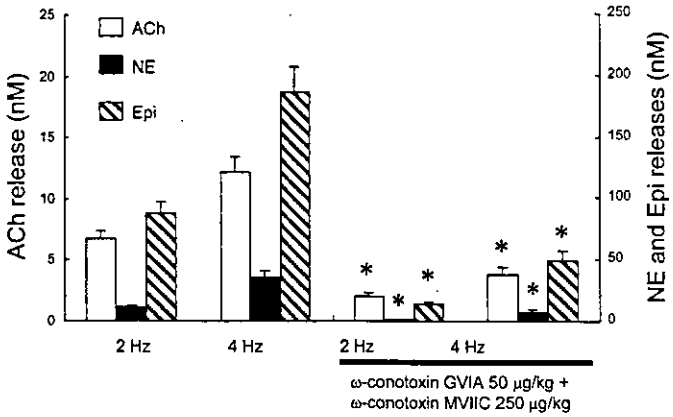

Fig. 3. Effects of combined ω-conotoxin GVIA and MVIIC on ACh, NE, and Epi releases. Combined ω-conotoxin GVIA (50 μg/kg) and MVIIC (250 μg/kg) inhibited ACh, NE, and Epi releases at 2 and 4 Hz. Values are means ± SE from 6 rats. $*P < 0.05$ vs. ACh, NE, or Epi release at same frequency before administration.

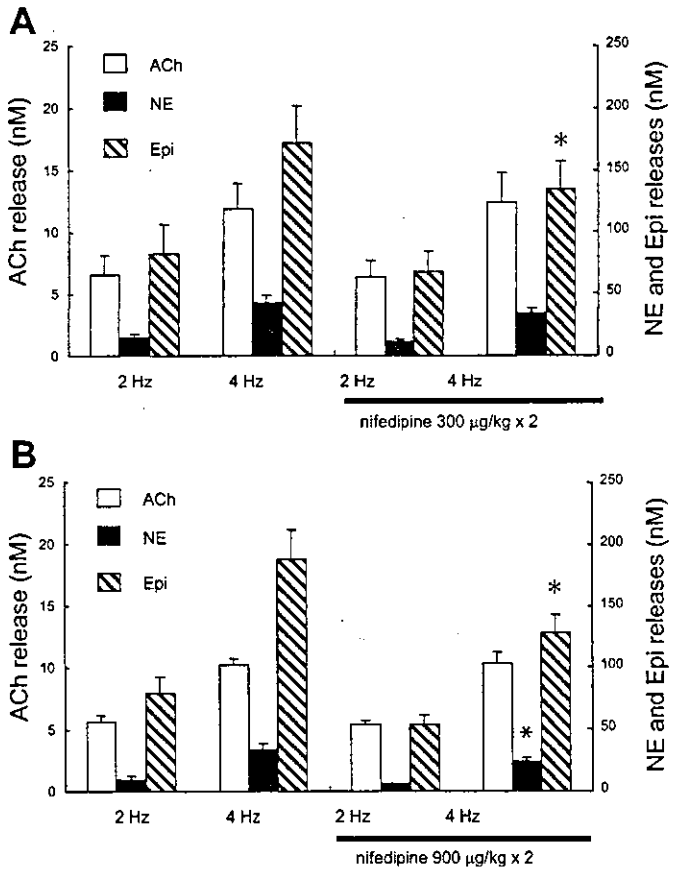

Fig. 4. Effects of nifedipine on ACh, NE, and Epi releases. Nifedipine (300 μg/kg) did not change ACh release at either frequency but inhibited Epi release at 4 Hz (*A*). Nifedipine (900 μg/kg) did not change ACh release at either frequency but inhibited NE and Epi releases at 4 Hz (*B*). Values are means ± SE from 6 rats. $*P < 0.05$ vs. ACh, NE, or Epi release at same frequency before administration.

endings or not play a major role in ACh release. This is the first direct study to demonstrate the type of Ca^{2+} channels controlling ACh release from splanchnic nerve endings.

In isolated rat adrenal glands, catecholamine release induced by field stimulation is sensitive to P/Q-type Ca^{2+} channel antagonist, whereas that induced by exogenous ACh is insensitive (27). This indirect study suggested the involvement of P/Q-type Ca^{2+} channels in ACh release but failed to show the involvement of N-type Ca^{2+} channels. In isolated bovine adrenal glands, a direct measurement study showed that a reduction of the extracellular Ca^{2+} concentration inhibits ^{3}H-labeled ACh release induced by field stimulation, but N- and L-type Ca^{2+} channel antagonists do not (28). Thus our findings are in part consistent with these direct and indirect studies but inconsistent as to the involvement of N-type Ca^{2+} channels.

This discrepancy might be ascribed to the experimental method. The contribution of Ca^{2+} channels may vary with the type of method used to evoke ACh release. In these studies, ACh release was evoked by electrical field stimulation of isolated adrenal glands, which is known to induce ACh release but not direct depolarization of chromaffin cells (34). In the present study, ACh release was evoked in the in vivo state by electrical stimulation of splanchnic nerves. The type of Ca^{2+} channels involved in ACh release may vary with the frequency, amplitude, or time period of stimulation. Actually, in the present study, we observed the involvement of P/Q-type Ca^{2+} channels at only high-frequency stimulation, while it has been reported in perfused rat adrenal glands that N-type Ca^{2+} channels are involved in the maintenance of catecholamine release in response to long splanchnic nerve stimulation (31). The time period of 2 min in the present study seems to be longer than those in earlier studies but could be within the physiological range. Moreover, the blocking action of ω-conotoxin GVIA is time dependent as well as dose dependent and irreversible (8, 11, 32, 36). The maximum functional effect of ω-conotoxin GVIA has been observed to be at least 15 min after administration. We evaluated the effect of ω-conotoxin GVIA 30 min after intravenous administration, when heart rate and mean arterial pressure had already been stabilized. The evaluation early after administration might lead to underestimation of the inhibitory effects of ω-conotoxin GVIA.

There are many similarities between synaptic transmission from splanchnic nerves to chromaffin cells and sympathetic ganglionic transmission (17). In isolated guinea pig paravertebral ganglia, an electrophysiological study has shown that both N- and P-type Ca^{2+} channel antagonists reduce cholinergic synaptic conductance, whereas L-type Ca^{2+} channel antagonist does not (19). In isolated rat superior cervical ganglia, both N- and P-type Ca^{2+} channel antagonists inhibit the rise in Ca^{2+} concentration in the terminal boutons (22). Moreover, in isolated rat superior cervical ganglia, ^{3}H-labeled ACh release induced by high K^+ is inhibited by both N- and P-type Ca^{2+} channel antagonists but unaffected by L-type Ca^{2+} channel antagonist (15). Our findings are similar to these findings obtained from isolated sympathetic preganglionic nerves.

The inhibition by ω-conotoxin GVIA (50 μg/kg) was almost the same as that by ω-conotoxin GVIA (10 μg/kg). Moreover, the inhibition by combined ω-conotoxin GVIA (50 μg/kg) and MVIIC (250 μg/kg) was almost algebraically the sum of the individual inhibition by ω-conotoxin GVIA (10 μg/kg) and MVIIC (50 μg/kg). These results suggest that fivefold higher doses of ω-conotoxin GVIA and MVIIC are sufficient to cause inhibition of Ca^{2+} channels. However, ~30% of ACh release was resistant to combined ω-conotoxin GVIA (50 μg/kg) and MVIIC (250 μg/kg). Other types of Ca^{2+} channels except for N- and P/Q-types may be involved in ACh release from splanchnic nerve endings. Further examination could be needed.

Effects of Ca^{2+} channel antagonists on catecholamine release from chromaffin cells. In the present study, nifedipine (300 μg/kg) did not change ACh release at 2 and 4 Hz but inhibited Epi release at 4 Hz by ~20%. A threefold higher dose of nifedipine (900 μg/kg) did not change ACh release at 2 and 4 Hz but inhibited NE and Epi releases at 4 Hz by ~30%. Adrenal chromaffin cells are divided into two populations: NE- and Epi-storing cells (10). L-type Ca^{2+} channels could be present on the surface of both NE- and Epi-storing cells and play a role in NE and Epi releases.

Approximately 70% of catecholamine release was resistant to nifedipine (900 μg/kg). This result suggests that other types of Ca^{2+} channels except for L-type are present on chromaffin cells and involved in NE and Epi releases, although we cannot exclude the possibility of incomplete inhibition of L-type Ca^{2+} channels. Species differences in the types of Ca^{2+} channels controlling Ca^{2+} influx and catecholamine release have been

shown with rat, cat, and bovine chromaffin cells (5, 6, 13, 24). In patch-clamp studies of isolated rat chromaffin cells, Ca^{2+} inward current elicited by depolarization is sensitive to both L- and N-type Ca^{2+} channel antagonists (16, 21). The study measuring Ba^{2+} current by patch-clamp technique has shown the existence of L-, N-, and P/Q-type Ca^{2+} channels on rat chromaffin cells and the following distribution of Ca^{2+} channels in decreasing order: L-type > N-type > P/Q-type (13). In the present study, ω-conotoxin GVIA (10 and 50 μg/kg) inhibited NE release at 4 Hz and Epi release at 2 and 4 Hz by approximately 45–50%. ω-Conotoxin MVIIC (50 μg/kg) inhibited Epi release at 4 Hz by ~30%. Combined ω-conotoxin GVIA (50 μg/kg) and MVIIC (250 μg/kg) inhibited NE and Epi releases at 2 and 4 Hz by approximately 75–85%. However, these Ca^{2+} channel antagonists simultaneously inhibited ACh release to almost the same extent. It is difficult to determine how much Ca^{2+} antagonists are acting on chromaffin cells when Ca^{2+} channel antagonists inhibit ACh release. Thus, although much of these inhibitions of catecholamine release may be considered to be consequences of the inhibition of ACh release, we cannot exclude the possibility that N- or P/Q-type Ca^{2+} channels may be involved in the in vivo catecholamine release on chromaffin cells.

The inhibition of NE release at 2 Hz by ω-conotoxin GVIA (10 and 50 μg/kg) and the inhibition of NE release at 4 Hz by ω-conotoxin MVIIC (50 μg/kg) were not statistically significant despite significant inhibitions of ACh and Epi releases. In the same preparation, we have shown that cholinergic antagonists almost inhibited NE and Epi releases induced by nerve stimulation (1, 2). However, the correlation between ACh and NE releases was poorer than that between ACh and Epi releases when stimulation frequency was raised stepwise (2). Insignificant inhibitions of NE release may be ascribed to this poor correlation.

In the present study, Ca^{2+} channel antagonists did not affect basal dialysate NE and Epi levels. In our previous study of the same preparation, these basal levels were not affected by neostigmine, hexamethonium, or atropine (1). We then concluded that these basal dialysate NE and Epi levels reflect noncholinergic catecholamine release. N-, P/Q-, and L-type Ca^{2+} channels may not play a major role in basal noncholinergic catecholamine release from adrenal medulla.

Methodological considerations. We administered neostigmine locally to adrenal medulla through a dialysis probe. Cholinesterase inhibitor was necessary to monitor endogenous ACh even during splanchnic nerve stimulation because released ACh is rapidly degraded by acetylcholinesterase before reaching the dialysis fiber. In the same preparation, local administration of neostigmine enhanced the dialysate catecholamine response to nerve stimulation by approximately threefold, but dialysate ACh and catecholamine responses are correlated with the stimulation frequency of splanchnic nerves in the presence of neostigmine (2). Thus dialysate ACh and catecholamine responses are likely to be correlated with the amount of Ca^{2+} influx from voltage-dependent Ca^{2+} channels even in the presence of neostigmine.

Intravenous administration of Ca^{2+} channel antagonists induced changes in heart rate or mean arterial pressure. These changes might affect ACh and catecholamine releases through a baroreflex mechanism. Moreover, these hemodynamic changes might decrease the spillover of ACh or catecholamine from adrenal medulla and affect the dialysate ACh or catecholamine concentrations (20). In our preparation, however, splanchnic nerves had been transected before control sampling, and basal dialysate catecholamine concentrations did not change before or after administration. Thus effects of these hemodynamic changes could be negligible when we considered the effects of Ca^{2+} channel antagonists on nerve stimulation-induced dialysate responses.

In conclusion, we applied dialysis technique to the adrenal medulla of anesthetized rats and investigated the effects of Ca^{2+} channel antagonists on ACh and catecholamine releases induced by electrical stimulation of splanchnic nerves. Both N- and P/Q-type Ca^{2+} channels control ACh release on preganglionic splanchnic nerve endings while L-type Ca^{2+} channels do not. L-type Ca^{2+} channels are involved in norepinephrine and epinephrine releases on chromaffin cells.

GRANTS

This study was supported by the Program for Promotion of Fundamental Studies in Health Science of the Organization for Pharmaceutical Safety and Research (of Japan); by a Health Sciences Research Grant for Advanced Medical Technology from the Ministry of Health and Welfare of Japan; by a Ground-Based Research Grant for the Space Utilization promoted by the National Space Development Agency of Japan and Japan Space Forum; and by grants-in-aid for scientific research from the Ministry of Education, Science.

REFERENCES

1. **Akiyama T, Yamazaki T, Mori H, and Sunagawa K.** Inhibition of cholinesterase elicits muscarinic receptor-mediated synaptic transmission in the rat adrenal medulla. *Auton Neurosci* 107: 65–73, 2003.
2. **Akiyama T, Yamazaki T, Mori H, and Sunagawa K.** Simultaneous monitoring of acetylcholine and catecholamine release in the in vivo rat adrenal medulla. *Neurochem Int* 44: 497–503, 2004.
3. **Akiyama T, Yamazaki T, and Ninomiya I.** In vivo detection of endogenous acetylcholine release in cat ventricles. *Am J Physiol Heart Circ Physiol* 266: H854–H860, 1994.
4. **Akiyama T, Yamazaki T, and Ninomiya I.** In vivo monitoring of myocardial interstitial norepinephrine by dialysis technique. *Am J Physiol Heart Circ Physiol* 261: H1643–H1647, 1991.
5. **Albillos A, Artalejo AR, López MG, Gandía L, García AG, and Carbone E.** Calcium channel subtypes in cat chromaffin cells. *J Physiol* 477: 197–213, 1994.
6. **Artalejo CR, Perlman RL, and Fox AP.** ω-Conotoxin GVIA blocks a Ca^{2+} current in bovine chromaffin cells that is not of the "classic" N type. *Neuron* 8: 85–95, 1992.
7. **Buckingham RE.** Studies on the anti-vasoconstrictor activity of BRL 34915 in spontaneously hypertensive rats; a comparison with nifedipine. *Br J Pharmacol* 93: 541–552, 1988.
8. **Clasbrummel B, Osswald H, and Illes P.** Inhibition of noradrenaline release by ω-conotoxin GVIA in the rat tail artery. *Br J Pharmacol* 96: 101–110, 1989.
9. **Coupland RE.** *The Natural History of the Chromaffin Cell.* London: Longmans, 1965.
10. **Coupland RE.** Ultrastructural features of the mammalian adrenal medulla. In: *Ultrastructure of Endocrine Cells and Tissues,* edited by Motta PM. Boston, MA: Nijhoff, 1984, p. 168–179.
11. **De Luca A, Li CG, Rand MJ, Reid JJ, Thaina P, and Wong-Dusting HK.** Effects of ω-conotoxin GVIA on autonomic neuroeffector transmission in various tissues. *Br J Pharmacol* 101: 437–447, 1990.
12. **Dunlap K, Luebke JI, and Turner TJ.** Exocytotic Ca^{2+} channels in mammalian central neurons. *Trends Neurosci* 18: 89–98, 1995.
13. **Gandía L, Borges R, Albillos A, and García AG.** Multiple calcium channel subtypes in isolated rat chromaffin cells. *Pflügers Arch* 430: 55–63, 1995.
14. **Gaspo R, Yamaguchi N, and de Champlain J.** Nifedipine inhibits adrenal but not circulating catecholamine response to nicotinic stimulation in dogs. *Am J Physiol Regul Integr Comp Physiol* 267: R1545–R1551, 1994.
15. **Gonzalez Burgos GR, Biali FI, Cherksey BD, Sugimori M, Llinas RR, and Uchitel OD.** Different calcium channels mediate transmitter release

evoked by transient or sustained depolarization at mammalian sympathetic ganglia. *Neuroscience* 64: 117–123, 1995.
16. **Hollins B and Ikeda SR.** Inward currents underlying action potentials in rat adrenal chromaffin cells. *J Neurophysiol* 76: 1195–1211, 1996.
17. **Holman ME, Coleman HA, Tonta MA, and Parkington HC.** Synaptic transmission from splanchnic nerves to the adrenal medulla of guinea-pigs. *J Physiol* 478: 115–124, 1994.
18. **Hillyard DR, Monje VD, Mintz IM, Bean BP, Nadasdi L, Ramachandran J, Miljanich G, Azimi-Zoonooz A, McIntosh JM, Cruz LJ, Imperial JS, and Olivera BM.** A new Conus peptide ligand for mammalian presynaptic Ca^{2+} channels. *Neuron* 9: 69–77, 1992.
19. **Ireland DR, Davies PJ, and McLachlan EM.** Calcium channel subtypes differ at two types of cholinergic synapse in lumbar sympathetic neurones of guinea-pigs. *J Physiol* 514: 59–69, 1999.
20. **Kawada T, Yamazaki T, Akiyama T, Shishido T, Inagaki M, Uemura K, Miyamoto T, Sugimachi M, Takaki H, and Sunagawa K.** In vivo assessment of acetylcholine-releasing function at cardiac vagal nerve terminals. *Am J Physiol Heart Circ Physiol* 281: H139–H145, 2001.
21. **Kim SJ, Lim W, and Kim J.** Contribution of L- and N-type calcium currents to exocytosis in rat adrenal medullary chromaffin cells. *Brain Res* 675: 289–296, 1995.
22. **Lin YQ, Brain KL, and Bennett MR.** Calcium in sympathetic boutons of rat superior cervical ganglion during facilitation, augmentation and potentiation. *J Auton Nerv Syst* 73: 26–37, 1998.
23. **Lomax RB, Michelrna P, Núñez L, García-Sancho J, García AG, and Montiel C.** Different contributions of L- and Q-type Ca^{2+} channels to Ca^{2+} signals and secretion in chromaffin cell subtypes. *Am J Physiol Cell Physiol* 272: C476–C484, 1997.
24. **López MG, Albillos A, de la Fuente MT, Borges R, Gandía L, Carbone E, García AG, and Artalejo AR.** Localized L-type calcium channels control exocytosis in cat chromaffin cells. *Pflügers Arch* 427: 348–354, 1994.
25. **Meir A, Ginsburg S, Butkevich A, Kachalsky SG, Kaiserman I, Ahdut R, Demirgoren S, and Rahamimoff R.** Ion channels in presynaptic nerve terminals and control of transmitter release. *Physiol Rev* 79: 1019–1088, 1999.
26. **Morimoto H, Matsuda A, Ohori M, and Fujii T.** Effects of ω-conotoxin GVIA on the activation of capsaicin-sensitive afferent sensory nerves in guinea pig airway tissues. *Jpn J Pharmacol* 71: 161–166, 1996.
27. **Nagayama T, Matsumoto T, Kuwakubo F, Fukushima Y, Yoshida M, Suzuki-Kusaba M, Hisa H, Kimura T, and Satoh S.** Role of calcium channels in catecholamine secretion in the rat adrenal gland. *J Physiol* 520: 503–512, 1999.
28. **O'Farrell M, Ziogas J, and Marley PD.** Effects of N- and L-type calcium channel antagonists and (±)-Bay K8644 on nerve-induced catecholamine secretion from bovine perfused adrenal glands. *Br J Pharmacol* 121: 381–388, 1997.
29. **Pruneau D and Belichard P.** Haemodynamic and humoral effects of ω-conotoxin GVIA in normotensive and spontaneously hypertensive rats. *Eur J Pharmacol* 211: 329–335, 1992.
30. **Randall A and Tsien RW.** Pharmacological dissection of multiple types of Ca^{2+} channel currents in rat cerebellar granule neurons. *J Neurosci* 15: 2995–3012, 1995.
31. **Santana F, Michelena P, Jaén R, García AG, and Borges R.** Calcium channel subtypes and exocytosis in chromaffin cells: a different view from the intact rat adrenal. *Naunyn Schmiedebergs Arch Pharmacol* 360: 33–37, 1999.
32. **Serone AP and Angus JA.** Role of N-type calcium channels in autonomic neurotransmission in guinea-pig isolated left atria. *Br J Pharmacol* 127: 927–934, 1999.
33. **Smith AB and Cunnane TC.** Multiple calcium channels control neurotransmitter release from rat postganglionic sympathetic nerve terminals. *J Physiol* 499: 341–349, 1997.
34. **Wakade AR.** Studies on secretion of catecholamines evoked by acetylcholine or transmural electrical stimulation of the rat adrenal gland. *J Physiol* 313: 463–480, 1981.
35. **Winer BJ.** *Statistical Principles in Experimental Design* (2nd ed.). New York: McGraw-Hill, 1971.
36. **Wright CE and Angus JA.** Prolonged cardiovascular effects of the N-type Ca^{2+} channel antagonist omega-conotoxin GVIA in conscious rabbits. *J Cardiovasc Pharmacol* 30: 392–399, 1997.
37. **Yahagi N, Akiyama T, and Yamazaki T.** Effects of ω-conotoxin GVIA on cardiac sympathetic nerve function. *J Auton Nerv Syst* 68: 43–48, 1998.

Am J Physiol Heart Circ Physiol 287: H196–H202, 2004.
First published March 4, 2004; 10.1152/ajpheart.00948.2003.

Single cell mechanics of rat cardiomyocytes under isometric, unloaded, and physiologically loaded conditions

Satoshi Nishimura,[1] So-ichiro Yasuda,[1] Masayoshi Katoh,[1] Kelly P. Yamada,[2] Hiroshi Yamashita,[1] Yasutake Saeki,[3] Kenji Sunagawa,[4] Ryozo Nagai,[1] Toshiaki Hisada,[2] and Seiryo Sugiura[2]

[1]*Department of Cardiovascular Medicine, Graduate School of Medicine, and* [2]*Biomechanics Division, Institute of Environmental Studies, Graduate School of Frontier Sciences, University of Tokyo, Tokyo 113-0033;* [3]*Department of Physiology, School of Dental Medicine, Tsurumi University, Kanagawa 230-5801; and* [4]*Department of Cardiovascular Dynamics, National Cardiovascular Center Research Institute, Osaka 565-8565, Japan*

Submitted 10 October 2003; accepted in final form 2 March 2004

Nishimura, Satoshi, So-ichiro Yasuda, Masayoshi Katoh, Kelly P. Yamada, Hiroshi Yamashita, Yasutake Saeki, Kenji Sunagawa, Ryozo Nagai, Toshiaki Hisada, and Seiryo Sugiura. Single cell mechanics of rat cardiomyocytes under isometric, unloaded, and physiologically loaded conditions. *Am J Physiol Heart Circ Physiol* 287: H196–H202, 2004. First published March 4, 2004; 10.1152/ajpheart.00948.2003.—One of the most salient characteristics of the heart is its ability to adjust work output to external load. To examine whether a single cardiomyocyte preparation retains this property, we measured the contractile function of a single rat cardiomyocyte under a wide range of loading conditions using a force-length measurement system implemented with adaptive control. A pair of carbon fibers was used to clamp the cardiomyocyte, attached to each end under a microscope. One fiber was stiff, serving as a mechanical anchor, while the bending motion of the compliant fiber was monitored for force-length measurement. Furthermore, by controlling the position of the compliant fiber using a piezoelectric translator based on adaptive control, we could change load dynamically during contractions. Under unloaded conditions, maximal shortening velocity was 106 ± 8.9 μm/s (n = 13 cells), and, under isometric conditions, peak developed force reached 5,720 nN (41.6 ± 5.6 mN/mm^2; n = 17 cells). When we simulated physiological working conditions consisting of an isometric contraction, followed by shortening and relaxation, the average work output was 828 ± 123 J/m^3 (n = 20 cells). The top left corners of tension-length loops obtained under all of these conditions approximate a line, analogous to the end-systolic pressure-volume relation of the ventricle. All of the functional characteristics described were analogous to those established by studies using papillary muscle or trabeculae preparations. In conclusion, the present results confirmed the fact that each myocyte forms the functional basis for ventricular function and that single cell mechanics can be a link between subcellular events and ventricular mechanics.

cardiomyocyte; mechanics; carbon fiber

SINGLE CARDIOMYOCYTE PREPARATIONS have been widely used to establish a link between subcellular molecular events and functional characteristics of the heart in the field of basic physiology (2, 3, 11, 23) and also for the evaluation of genetic modification of myocytes (8, 17). The simple geometry of a single cell offers great advantages over multicellular preparations due to uniformity in myofibril alignment and stress-strain distribution as well as homogeneous distribution of exogenous indicators or gene products. On the other hand, irritability of the sarcolemma devoid of collagen matrix makes cell attachment to the experimental apparatus difficult, thereby disturbing measurements of force, stiffness, and shortening velocity under a variety of loading and perturbational conditions. Thus existing methods were unable to provide a complete description of the mechanical component of the contractile process that can be related to underlying biochemical processes (3).

To overcome this problem, we have already reported a novel force measurement system for a single cardiomyocyte (26) in which carbon fibers enabled the stable recording of force with minimal requirements for technical skill. In addition, feedback control of fiber movement permitted the study of mechanics of a single cardiomyocyte under isometric as well as unloaded shortening conditions (25). Application of this method at the two extremes of loading conditions provided us with a unique opportunity to study the load dependence of contraction characteristics. The behavior of cardiomyocytes as they are in the wall of working heart is different. During the cardiac cycle, each cardiomyocyte in the ventricular wall faces varying loading conditions to trace a force-length loop analogous to the pressure-volume loops of the ventricles. Both experimental (13) and simulation studies (21, 22) of cardiomyocytes suggest considerable variations exist in the shape of force-length loops within the ventricular wall and under different loading conditions. To our knowledge, no study has reported such force-length loops and their characteristics of a single cardiomyocyte in vitro.

In this study, we succeeded in recording single cardiomyocyte contraction mechanics under physiological loading conditions and compared findings with those under isometric and unloaded conditions as well as under inotropic intervention in the same myocyte. Because noise in length signals hampered real-time feedback control, we adopted an adaptive control strategy in combination with digital filtering of the signal. The results are shown together with the simultaneous recording of sarcomere length to indicate the potential of this method in linking the cardiac function at molecular, cellular, and ventricular levels.

METHODS

Cell isolation. All studies were conducted in accordance with the National Institutes of Health *Guide for the Care and Use of Laboratory Animals* and were approved by the Institutional Animal Care and Use Committee. Single ventricular myocytes were enzymatically

Address for reprint requests and other correspondence: S. Sugiura, Biomechanics Div., Institute of Environmental Studies, Graduate School of Frontier Sciences, Univ. of Tokyo, Bunkyo-ku, Tokyo 113-0033, Japan (E-mail: sugiura@k.u-tokyo.ac.jp).

The costs of publication of this article were defrayed in part by the payment of page charges. The article must therefore be hereby marked "*advertisement*" in accordance with 18 U.S.C. Section 1734 solely to indicate this fact.

isolated using a modified dispersion technique that has been described previously (9). Briefly, the heart was quickly removed from male Wistar rats (7–10 wk old) under pentobarbital anesthesia. Retrograde perfusion was performed with Ca^{2+}-free HEPES-Tyrode solution [containing (in mM) 137 NaCl, 5.4 KCl, 1.8 $CaCl_2$, 0.5 $MgCl_2$, 0.33 NaH_2PO_4, 5 HEPES, and 5 glucose; pH 7.4 adjusted by NaOH at 37°C] for 5 min, followed by an enzyme solution containing collagenase (0.4 mg/ml collagenase S-1, Nitta gelatin), protease (0.08 mg/ml, type XIV, Sigma), and 0.1 mM Ca^{2+} for 3.5 min. The ventricular tissue was then cut into small pieces and filtered with 200-μm nylon mesh. The calcium concentration of Tyrode solution was gradually increased to 1.1 mM, and the myocytes were transferred to the experimental chamber. The glass bottom of the chamber was coated with 2-hydroxyethyl methacrylate (Sigma) to prevent adhesion of cells.

Force-length measurements. The basic principle of the single cardiomyocyte force-length measurement system has been described previously (25, 26). In each experiment, a single cardiomyocyte was selected under a microscope according to the following criteria: *1*) rod-shaped cell with average sarcomere length > 1.65 μm (measured by on-line Fourier analysis of optical density traces of the sarcomere pattern of a myocyte image, SarcLen, IonOptix; Milton, MA); and *2*) responded to electrical stimulation to contract over 5% of the total cell length. To each end of the selected myocyte, we attached a carbon fiber using micromanipulators. One of the fibers was compliant (diameter 7 μm, length 1–1.2 mm, stiffness 80–200 nN/μm), whereas the other thick one was rigid (diameter 30 μm, length ≈1 mm, stiffness > 1,000 nN/μm), serving as a mechanical anchor. They were made from a mixture of fine graphite granules and resin oligomer and made by shaping into rods by thrusting through a thin hole in a block of sapphire (26). The image of the compliant fiber was projected onto a linear 1,024-element photodiode array (S3903, Hamamatsu Photonics) for monitoring its bending motion induced by active contraction or passive stretch. Furthermore, we controlled the position of the compliant fiber by moving the piezoelectric translator (PZT; P-841.40, Physik Instrumente) connected to it (Fig. 1). The cell was electrically stimulated at 0.5 Hz with pulses of 10-ms duration. Before force measurement, we stretched the diastolic cell length to 105% of the slack length while measuring sarcomere length (IonOptix). Streptomycin sulphate (10 μg/ml, Sigma) was added to the Tyrode solution to prevent stretch-induced arrythmia. All experiments were performed at 37°C (Thermoplate, TOKAIHIT).

Estimation of force. The stiffness of the carbon fiber was determined by pushing it against a glass fiber of known stiffness (27). The stiffness thus determined agreed well with the theoretical value (K) for a beam with a circular cross section derived from the following equation:

$$K = \frac{3 \cdot \pi \cdot E \cdot D^4}{64 \cdot l^3} \quad (1)$$

where D is the diameter of the fiber (7 μm), l is the length of the fiber (1–1.2 mm), and E is Young's modulus of carbon (≈0.39 N/μm²). All previous studies including ours (16, 23, 25, 26) have used this stiffness value assuming that the cardiomyocyte applies concentrated lateral load to the free end of the cantilever beam (APPENDIX, *Case A*). However, the following experimental observations led us to consider an alternative model for the fiber displacement in which a bending moment is applied to the tip of the beam (APPENDIX, *Case B*): *1*) the load was not concentrated at the tip because the myocyte attaches the fiber along its width; and *2*) the myocyte shortened while always retaining its straight shape. We have examined the validity of models by closely monitoring the shape of the fiber while it was bent by motion of the myocyte. We measured the displacement of the fiber at multiple points from the tip of the fiber by shifting the photodiode array sensor along the image of the fiber during contraction. As shown in Fig. 2, we plotted the measured displacement (normalized by the displacement at the tip) and compared it with the predictions by *cases A* and *B* in the APPENDIX. In proximity to the tip, the carbon fiber moved in a parallel manner (without rotation) because of its firm attachment to the myocyte and its displacement was close to the prediction by *case B*. This result indicated that a bending moment was applied to the tip of the beam and thus must be taken into account for analysis (APPENDIX, *Case B*). Accordingly, we used the effective stiffness (K') defined as follows (see the APPENDIX) for the estimation of force:

$$K' = \frac{12 \cdot \pi \cdot E \cdot D^4}{64 \cdot l^3} = 4 \cdot K \quad (2)$$

In this analysis, force (F) was calculated as

$$F = K' \cdot (x - y) \quad (3)$$

where x is the shortening length of the myocyte and y is the displacement of the PZT.

Digital control of the system. To enhance the ability of the system to achieve working conditions of a single myocyte, we replaced the analog circuit (26) with a personal computer (PC)-based digital control system. Cell length signals obtained by the photodiode array sensor were sampled and processed at 1 kHz, and the generated command signal was applied to the PZT driver with a 16-bit analog-to-digital, digital-to-analog converter (6035E, National Instruments) connected to the PC. We adopted a two-stage adaptive control strategy (19). During the preparation stage, which consisted of five paced contractions, the PZT was held at the neutral position to obtain the baseline force-length history. Next, in the adaptation stage, the command signal (y) was calculated from x and F of the preceding contraction. To obtain the isometric condition ($x = 0$), the error signal in the ith contraction was $x_i - 0 (= x_i)$. Thus the command signal for the next contraction would be

$$y_{i+1} = y_i + A \cdot x_i \quad (4)$$

where A is a negative constant. Similarly, for an unloaded shortening contraction (F = 0), command for the $(i + 1)$th contraction would be

$$y_{i+1} = y_i + A \cdot \frac{F_i}{K'} \quad (5)$$

where F_i is calculated by *Eq. 3* and A is a constant. With an empirically determined A value, y_i converged within three or four contractions, and measurement was performed in the next contraction. We simulated the physiological loading sequence by switching the

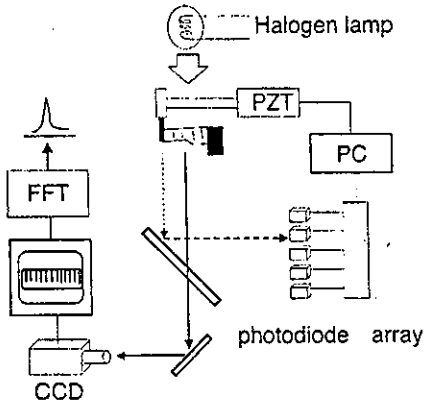

Fig. 1. Diagram of the experimental setup. Position of the fiber was detected by the photodiode array. The position signal was processed by a personal computer (PC), and the calculated command signal was applied to a piezoelectric translator (PZT) connected to the carbon fiber. The sarcomere pattern was captured by a charge-coupled device (CCD) camera, and sarcomere length was determined by fast Fourier transform (FFT).

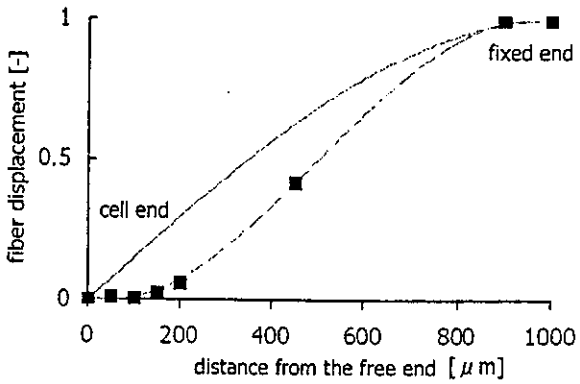

Fig. 2. Displacement of the carbon fiber induced by myocyte contraction. The experimental data (■) are compared with the predictions by *case A* (solid line) and *case B* (dashed line) in the APPENDIX. Displacement was normalized by the displacement at the tip.

control mode from isometric-isotonic contraction to isometric-auxotonic relaxation. When the myocyte was stimulated, myocyte length was held constant and isometric force developed. When the force reached a predetermined threshold, control mode was switched to isotonic and the myocyte was allowed to shorten. The myocyte length was then kept constant until the force became zero, and the myocyte was stretched to the original length under auxotonic length control.

We performed a single measurement for each protocol in each myocyte.

Data analysis. All data were sampled at 1 kHz and recorded by an analog-to-digital converter connected to a PC (MacLab 8s, ADInstruments). It is known that isolated cells, when placed in physiological medium, assume a cross-sectional area that resembles a flattened ellipse (1, 24). We measured the long and short axes of myocytes by rolling them using carbon fibers under a microscope and determined the average ratio between long and short axes as 3:1 in a different set of experiments (data not shown). The cross-sectional area of the myocyte was estimated from videotaped images assuming an elliptical cross section with this value. Results are expressed as means ± SE.

RESULTS

We succeeded in measuring force and length relations in 20 cells (Table 1). The mean cell length between two attached carbon fibers was 67.0 ± 2.5 μm, the cell width was 25.9 ± 1.36 μm, and the diastolic sarcomere length was 1.74 ± 0.01 μm before stretch was applied.

Load dependence of cardiomyocyte contraction. Figure 3 shows typical records of the length and force changes under isometric and unloaded conditions obtained from the same cardiomyocyte. Under isometric conditions, the shortening length was <0.5 μm and the peak force was 5,720 nN (41.6 ± 5.6 mN/mm^2; n = 17 cells), comparable to those obtained in papillary muscle preparations. Under unloaded conditions, cells shortened to 5.81 ± 0.27 μm (n = 18 cells), which was equal to 8.9% of the cell length under control (the segment between the fibers under resting conditions). The maximal shortening velocity was 106 ± 8.9 μm/s (n = 13 cells). Variability in the isometric force per unit cross-sectional area and percent shortening under unloaded conditions was fairly small, indicating the reproducibility of this experiment. The time course of contraction also showed a physiological response to load. That is, under isometric conditions, the duration of contraction shortened and the time to peak force was also decreased, as shown in Fig. 3.

We succeeded in achieving the ejecting mode of contraction in 20 cells. The achieved physiological work loops in 20 cells were similar to those reported in both experimental (13) and simulation studies (Fig. 4) (22). We calculated the external work using force per myocyte (raw data: N) and length (in m)

Table 1. *The contractile functions under unloaded, isometric, and physiologically loaded conditions for each myocyte studied*

	Shortening Under Unloaded Conditions			Force Under Isometric Conditions		Physiologically Loaded Conditions				
	Length, μm	Length, %	V_{max} μm/s	Force, μN	Force, mN/mm^2	Work area, J/m^3	Maximum force, μN	Shortening, μm	Shortening, %	Slope of Linear Regression, nN/μm
1	6.11	8.01	108	4.72	34.3	450	2.88	3.18	4.17	764
2	6.19	8.52	105	6.18	25.8	355	3.19	4.41	6.07	941
3	4.50	7.46		4.94	27.4	588	1.79	4.09	6.78	1,212
4	3.54	4.46		4.91	30.6	269	1.53	3.37	4.25	1,969
5	7.90	8.86				463	4.00	6.96	7.80	1,312
6	5.98	7.79		6.22	33.3	330	2.88	3.75	4.88	
7	5.63	11.02	89	6.50	33.5	1,177	3.30	4.64	9.09	1,248
8	5.00	7.89	67	4.98	24.8	439	2.53	4.68	7.38	1,059
9	3.97	5.83	58	3.88	18.6	323	1.87	3.86	5.67	1,101
10	5.88	7.60	109	4.34	36.6	1,131	2.67	5.37	6.95	925
11	7.00	8.65		4.27	32.9	690				2,275
12	4.69	7.91	89	4.27	36.0	1,530	3.88	3.98	6.71	1,566
13	6.40	9.85	97	9.08	38.0	1,140	5.40	5.98	9.21	1,730
14	5.15	8.76	90	4.54	57.8	901	1.98	3.68	6.26	523
15	6.18	12.11	114	7.84	60.3	1,555	3.30	4.58	8.97	809
16	6.81	13.62	168	5.85	45.1	1,281	3.63	4.64	9.28	1,214
17	6.47	11.95	136	5.34	49.5	1,119	3.50	5.12	9.46	1,280
18	7.25	10.99	159	9.52	121.2	2,235	4.51	5.08	7.70	1,472
19						227	2.20	3.97	5.79	
20						362	2.56	3.63	4.99	
Mean	5.81	8.96	106.8	5.72	41.6	828	3.03	4.55	6.92	1,259
SE	0.27	0.54	8.9	0.41	5.6	123	0.23	0.23	0.40	108

V_{max}, maximum velocity.

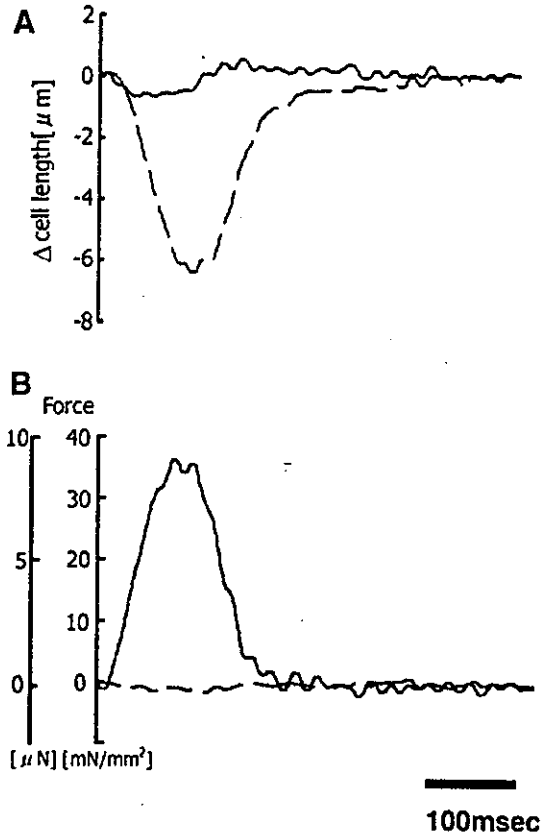

Fig. 3. Cell length and force during isometric and unloaded shortening contractions in the same myocyte. *A*: cell length during isometric (solid line) and unloaded shortening (dashed line) contractions. Length change during the isometric contraction was <0.5 μm. *B*: developed force during the isometric (solid line) and unloaded shortening (dashed line) contractions shown in *A*. During unloaded shortening, the force was zero. In this cell, cross-sectional area was 749 μm².

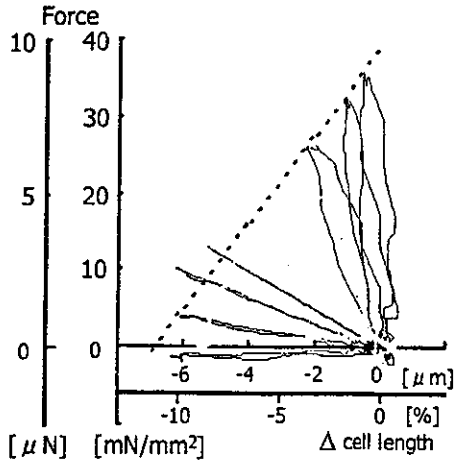

Fig. 4. Force-length loop of a single cardiomyocyte under various loading conditions. Data were obtained during adaptive control for isometric and unloaded shortening as well as simulated ejection. The *y*-axis shows force (raw data) and force per cross-sectional area (in this cell, cross-sectional area was 749 μm²). Linear regression was applied to the top left corner points of the loops. The slope of the regression line was 1,730 nN/μm. External work produced by the ejecting contraction was 1,139 J/m³.

data. The achieved physiological work calculated thus determined in 20 cells was 828 ± 123 J/m³.

We changed load and obtained a series of force-length loops. The curve connecting the top left corners of these loops was convex upward, analogous to the end-systolic pressure-volume relation of the rodent ventricle (Fig. 4) (12). Applying linear regression to these points yielded a slope of 1,260 ± 108 nN/μm (n = 17 cells).

By stretching the cells before the contraction, we could observe the effect of increasing preload. As shown in Fig. 5, not only the isometric force (Fig. 5*A*) and unloaded shortening length (data not shown) but also the external work (Fig. 5*B*) increased depending on the preload. Because muscle length and force at baseline varied considerably, we could not achieve statistical analysis of this findings, but similar preload dependence was found in 10 cells.

Sarcomere length. We measured sarcomere length and compared it with simultaneously recorded cell length. We confirmed that cell length always changed in parallel with sarcomere length under resting conditions as well as during contraction against low load (Fig. 6*A*). In 12 cells in which sarcomere length signals of good quality were obtained, similar observations were made. Although it was difficult to determine sarcomere length during isometric conditions due to blurring of the sarcomere pattern, we could record it in eight cells. Although small compared with sarcomere shortening during uncontrolled contraction under unloaded conditions (Fig. 6*B*, solid line), we observed internal shortening of sarcomeres (Fig. 6*B*, dashed line) of the same magnitude (≈0.1 μm) in 8 cells.

DISCUSSION

Single cell mechanics by the carbon fiber technique. In this study, we studied the mechanics of single rat cardiomyocytes over a wide range of loading conditions including isometric, unloaded, and physiological loading conditions. To our knowl-

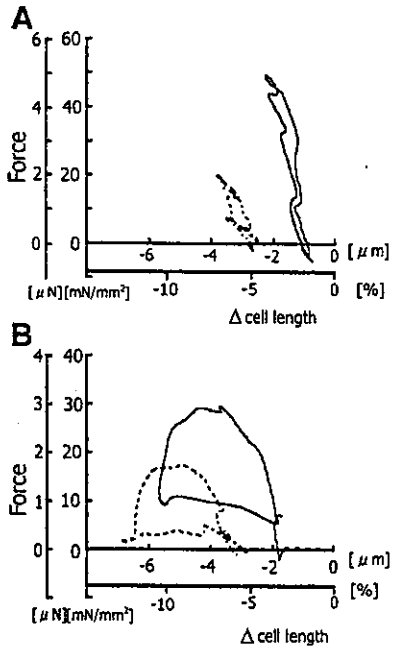

Fig. 5. Preload dependence of contractile function *A*: isometric contractions under two different (solid line 1.78 μm; dashed line 1.71 μm) preloads. *B*: ejecting contractions under two different preloads showing the preload dependence of external work. The *y*-axis shows force (raw data) and force per cross-sectional area (in this cell, cross-sectional area was 323 μm²).

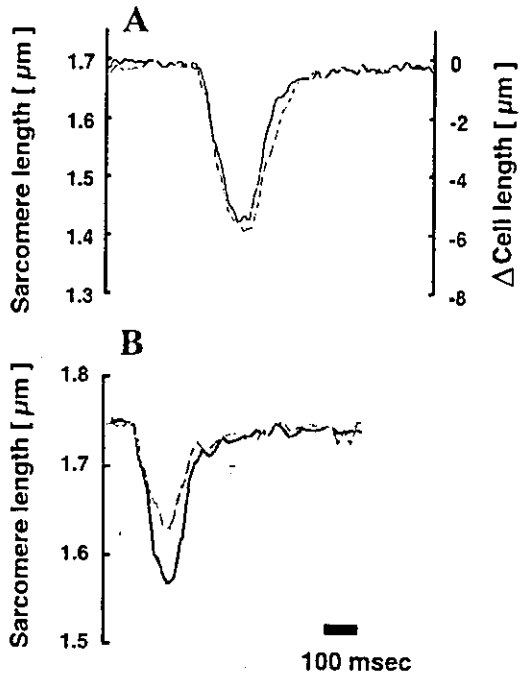

Fig. 6. Relationship between cell length and sarcomere length. *A*: simultaneous recording of cell length (solid line) and sarcomere length (dashed line) during contraction under unloaded conditions. *B*: sarcomere length during isometric contraction (dashed line) and under unloaded conditions (solid line) recorded in the same cell.

edge, this is the first time that physiological force-length loops have been reported in isolated myocytes. Because of its important role in relating subcellular molecular events to ventricular dynamics, many researchers have studied single cell mechanics of cardiomyocytes using various methods (11). Compared with other methodologies, the carbon fiber technique is superior in two aspects. First, it is relatively simple and does not require technical expertise. Second, attachment of carbon fibers results in minimal damage to the sarcolemma (11). With the use of carbon fibers (26), the overall success rate for establishing firm attachment to myocytes was over 80% in this series of experiments, and myocytes remained stable for 10 min of contractions by electric stimulation. This excellent stability enabled us to study myocyte mechanics under various loading conditions as well as under inotropic interventions in the same myocyte, which, in certain cases, was helpful in avoiding cell-to-cell variations. In addition, we obtained a peak isometric force of 5.72 μN in this study. This is in the highest range of twitch force reported so far [Ref. 3 and review by Bluhm et al. (2)] and is ≈75% of the maximally activated force (7.5 μN) (10) obtained in a single skinned rat cardiomyocyte, supporting its usefulness.

Physiological significance. In rat trabeculae preparations, Janssen and de Tombe (14) reported an isometric twitch force of 45 mN/mm^2 for muscle isometric twitches and 88.5 mN/mm^2 for sarcomere isometric twitches. In a left ventricular papillary muscle preparation, isometric force was ~6 g/mm^2 (≈60 mN/mm^2) (5). The isometric force obtained in this study (41.6 ± 5.6 mN/mm^2) was somewhat lower but close to these values. For shortening velocity, we obtained 106 ± 8.9 μm/s, which is equivalent to 1.58 lengths/s (37°C). In rat trabeculae, predominantly containing the V_1 myosin isoform, an unloaded shortening velocity of 2.3 lengths/s (30°C) has been reported (20). On the other hand, Josephson et al. (15) measured the maximal shortening velocity of euthyroid rat ventricular myocytes at 29°C and reported a value of 1.17 lengths/s. Again, our results are close to these values, suggesting that carbon fiber attachment does not create extra load if its movement is properly controlled as in this study. However, the key feature required for single cell mechanics is how accurately it can reproduce and describe the behavior of the cell in the body. In response to change in afterload, we obtained a series of force-length loops. The top left corners of these loops distributed along a straight line, analogous to the end-systolic pressure-volume relation of the ventricle (Fig. 4). Furthermore, when inotropic intervention was applied to a single myocyte by adding isoproterenol (2 μM) to the medium, the slope of this line increased in a similar manner with the ventricular end-systolic pressure-volume relation (Fig. 7, *A* and *B*). Preload dependence was also confirmed (Fig. 5). Finally, using digital control, we could obtain physiological force-length loops of a single cardiomyocyte (Fig. 4) resembling those reported in experimental (13) and simulation studies (21, 22). The average work output per unit volume calculated from the stress-relative shortening area was 828 ± 123 J/m^3. If we assume the density of cardiac muscle to be ~1g/cm^3, 1 g of the rat ventricle (cm^3) would generate 0.83 mJ. This value is ~13% of the external work done by a rat ventricle ejecting 500 μl of blood while generating ~100 mmHg. The cause of this discrepancy is not clear, but the lack of sympathetic stimulation to the isolated myocyte could be one of the possibilities.

Adaptive control of cell length and force. With the real-time analog control system we used in previous studies (25, 26), it

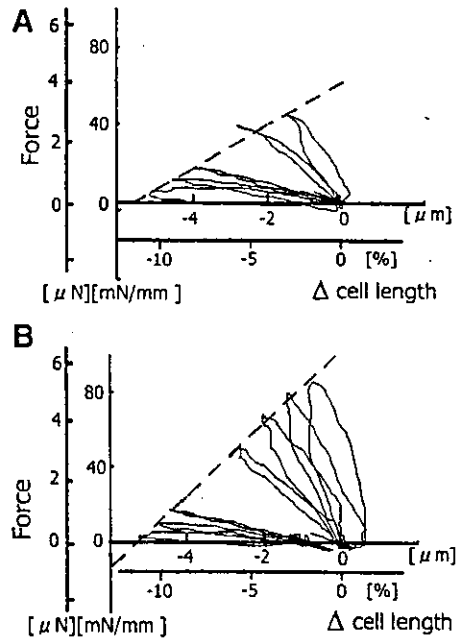

Fig. 7. Force-length relation of a single cardiomyocyte before (*A*) and after (*B*) the addition of isoproterenol (2 μM) to the medium. Isometric force increased from 44 to 85 mN/mm^2, and the slope of the regression line increased from 11 to 19 mN·mm^{-2}·μm^{-1}. The *y*-axis shows force (raw data) and force per cross-sectional area (in this cell, cross-sectional area was 197 μm^2).

was very difficult to achieve physiological loading largely because of noise in the length signal. Adaptive control, together with zero-delay low-pass filtering, avoided transmission and amplification of noise and successfully circumvented this problem. Furthermore, once the proper command signal could be obtained, the high-intensity illumination for photodiode sensors was not required, allowing the recording of calcium indicator fluorescence for a longer period of time without causing photobleaching.

Study limitations. The major concern with this attachment technique is to avoid damaging the ends of myocytes and to obtain uniform sarcomere spacing (18). Using real-time image analysis, we confirmed that static stretch applied to a resting myocyte could cause uniform stretch of the sarcomere in proportion to cell length. Because of the difficulty in keeping focus on the sarcomere, we could not accurately measure sarcomere length during isometric contractions. However, in the few cases where we could obtain the simultaneous recording of sarcomere length during isometric contraction, internal shortening did take place (Fig. 6*B*). To achieve precise control of sarcomere length, further improvement of the experimental setup may be necessary.

Finally, some myocytes were too irritable to obtain stable recordings, even with streptomycin in the medium as an inhibitor of stretch-activated channels. This might have lead to selection bias of myocytes and disturbed the experiment.

In summary, by adopting digital adaptive control, we studied the mechanics of a rat single cardiac myocyte over a wide range of loading conditions. All of the functional characteristics described were analogous to those established by a number of studies using papillary muscle (4, 6) or trabeculae preparations (7). The present results confirmed the fact that each myocyte forms the functional basis for ventricular function and that single cell mechanics can be a link between subcellular events and ventricular mechanics.

APPENDIX: RELATION BETWEEN LOAD AND LATERAL DISPLACEMENT OF A BEAM

Case A

When lateral force (P) applied to the free end of a cantilever beam [length (l)] causes displacement (y) (Fig. 8), they are related as

$$y = \frac{P \cdot l^3}{3 \cdot E \cdot I} \tag{A1}$$

or

$$P = \frac{3 \cdot E \cdot I}{l^3} \cdot y \tag{A2}$$

where I is the second moment of inertia of the cross section and E is Young's modulus.

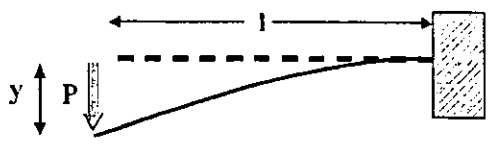

Fig. 8. *Case A.* Lateral force (P) applied to the free end of a cantilever beam [length (l)] causes displacement (y).

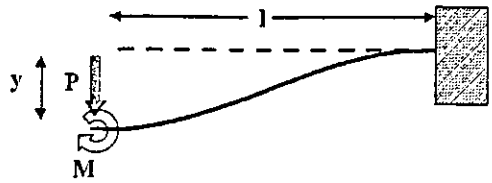

Fig. 9. *Case B.* For the end of fiber to move in parallel manner (without rotation), an appropriate amount of bending moment (M) should also be applied.

For a beam having a circular cross section with diameter D

$$P = \frac{3 \cdot \pi \cdot E \cdot D^4}{64 \cdot l^3} \cdot y \tag{A3}$$

Case B

For the end of fiber to move in parallel manner (without rotation), an appropriate amount of bending moment (M) should also be applied (Fig. 9). Such a load can be calculated as

$$M = \frac{P \cdot l}{2} \tag{A4}$$

The displacement (y') induced by M is

$$y' = -\frac{M \cdot l^2}{2 \cdot E \cdot I} \tag{A5}$$

Total displacement (y) caused by lateral load P and moment load M is then

$$y = \frac{P \cdot l^3}{3 \cdot E \cdot I} - \frac{P \cdot l^3}{4 \cdot E \cdot I} = \frac{P \cdot l^3}{12 \cdot E \cdot I} \tag{A6}$$

or

$$P = \frac{12 \cdot E \cdot I}{l^3} \cdot y \tag{A7}$$

Similarly, for a beam having a circular cross section with diameter D

$$P = \frac{12 \cdot \pi \cdot E \cdot D^4}{64 \cdot l^3} \cdot y \tag{A8}$$

In *case A*, the displacement y at x from the free end is calculated as

$$y = \frac{P}{6 \cdot E \cdot I}(x^3 - 3l^2x + 2l^3) \tag{A9}$$

or at the distance (z) from the fixed end as

$$y = \frac{P}{6 \cdot E \cdot I}z^2 \cdot (3l - z) \tag{A10}$$

In *case B*, the displacement y at x from the free end is calculated as

$$y = \frac{P}{12 \cdot E \cdot I}(l - x)^2 \cdot (l + 2x) \tag{A11}$$

or at z from the fixed end as

$$y = \frac{P}{12 \cdot E \cdot I}z^2 \cdot (3l - 2z) \tag{A12}$$

ACKNOWLEDGMENTS

We thank C. Miyazawa for excellent technical assistance.

GRANTS

This study was supported by grants from the Program for Promotion of Fundamental Studies in Health Sciences of the Organization for Pharmaceutical Safety Research, the Vehicle Racing Commemorative Foundation, the Fugaku Trust for Medical Research, and a Research Grant for Cardiovascular Disease from the Ministry of Health, Labor and Welfare. K. P. Yamada was supported by a Japan Society for the Promotion of Science postdoctoral fellowship for foreign researchers.

REFERENCES

1. **Anversa P and Olivetti G.** Cellular basis of physiological and pathological myocardial growth. In: *Handbook of Physiology. The Cardiovascular System. The Heart.* Bethesda, MD: Am. Physiol. Soc., 2000, sect. 2, vol. I, chapt. 2, p. 75–144.
2. **Bluhm WF, McCulloch AD, and Lew WY.** Active force in rabbit ventricular myocytes. *J Biomech* 28: 1119–1122, 1995.
3. **Brady AJ.** Mechanical properties of isolated cardiac myocytes. *Physiol Rev* 71: 413–428, 1991.
4. **Brady AJ, Tan ST, and Ricchiuti NV.** Contractile force measured in unskinned isolated rat heart fibers. *Nature* 282: 728–729, 1979.
5. **Brooks WW, Bing OH, Blaustein AS, and Allen PD.** Comparison of contractile state and myosin isoenzyme of rat right and left ventricular myocardium. *J Mol Cell Cardiol* 19: 433–440, 1987.
6. **Brutsaert DL and Sonnenblick EH.** Force-velocity-length-time relations of the contractile elements in heart muscle of the cat. *Circ Res* 24: 137–149, 1969.
7. **De Tombe PP and ter Keurs HEDJ.** Force and velocity of sarcomere shortening in trabeculae from rat heart. Effects of temperature. *Circ Res* 66: 1239–1254, 1990.
8. **Del Monte F, Harding SE, Schmidt U, Matsui T, Kang ZB, Dec GW, Gwathmey JK, Rosenzweig A, and Hajjar RJ.** Restoration of contractile function in isolated cardiomyocytes from failing human hearts by gene transfer of SERCA2a. *Circulation* 100: 2308–2311, 1999.
9. **Farmer BB, Mancina M, Williams ES, and Watanabe AM.** Isolation of calcium tolerant myocytes from adult rat hearts: review of the literature and description of a method. *Life Sci* 33: 1–18, 1983.
10. **Fitzsimons DP, Patel JR, and Moss RL.** Role of myosin heavy chain composition in kinetics of force development and relaxation in rat myocardium. *J Physiol* 513: 171–183, 1998.
11. **Garnier D.** Attachment procedures for mechanical manipulation of isolated cardiac myocytes: a challenge. *Cardiovasc Res* 28: 1958–1964, 1994.
12. **Georgakopoulos D and Kass DA.** Minimal force-frequency modulation of inotropy and relaxation of in situ murine heart. *J Physiol* 534: 535–545, 2001.
13. **Guccione JM, LePrell GS, de Tombe PP, and Hunter WC.** Measurement of active myocardial tension under a wide range of physiological loading conditions. *J Biomech* 30: 189–192, 1997.
14. **Janssen PM and de Tombe PP.** Uncontrolled sarcomere shortening increases intracellular Ca^{2+} transient in rat cardiac trabeculae. *Am J Physiol Heart Circ Physiol* 272: H1892–H1897, 1997.
15. **Josephson RA, Spurgeon HA, and Lakatta EG.** The hyperthyroid heart. An analysis of systolic and diastolic properties in single rat ventricular myoyctes. *Circ Res* 66: 773–781, 1990.
16. **Le Guennec JY, Peineau N, Argibay JA, Mongo KG, and Garnier D.** A new method of attachment of isolated mammalian ventricular myocytes for tension recording: length dependence of passive and active tension. *J Mol Cell Cardiol* 22: 1083–1093, 1990.
17. **Michele DE, Albayya FP, and Metzger JM.** Direct, convergent hypersensitivity of calcium-activated force generation produced by hypertrophic cardiomyopathy mutant alpha-tropomyosins in adult cardiac myocytes. *Nat Med* 5: 1413–1417, 1999.
18. **Palmer RE, Brady AJ, and Roos KP.** Mechanical measurement from isolated cardiac myocytes using a pipette attachment system. *Am J Physiol Cell Physiol* 270: C697–C704, 1996.
19. **Peterson JN, Hunter WC, and Berman MR.** Control of segment length or force in isolated papillary muscle: an adaptive approach. *Am J Physiol Heart Circ Physiol* 256: H1726–H1734, 1989.
20. **Regnier M, Lee DM, and Homsher E.** ATP analogs and muscle contraction: mechanics and kinetics of nucleotide tirphosphate binding and hydrolysis. *Biophys J* 74: 3044–3058, 1998.
21. **Stevens C and Hunter PJ.** Sarcomere length change in a 3D mathematical model of the pig ventricle. *Prog Biophys Mol Biol* 82: 229–241, 2003.
22. **Watanabe H, Hisada T, Sugiura S, Okada J, and Fukunari H.** Computer simulation of blood flow, left ventricular wall motion and their interrelationship by fluid-structure interaction finite element method. *JSME Int J* 44: 125–133, 2002.
23. **White E, Boyett MR, and Orchad CH.** The effects of mechanical loading and changes of length on single guinea-pig ventricular myocytes. *J Physiol* 482: 93–107, 1995.
24. **Wu Y, Cazorla O, Labeit D, Labeit S, and Granzier H.** Changes in titin and collagen underlie diastolic stiffness diversity of cardiac muscle. *J Mol Cell Cardiol* 32: 2151–2162, 2000.
25. **Yasuda S, Sugiura S, Yamashita H, Nishimura S, Saeki Y, Momomura S, Katoh K, Nagai R, and Sugi H.** Unloaded shortening increases the peak of Ca^{2+} transients but accelerates their decay in rat single cardiac myocytes. *Am J Physiol Heart Circ Physiol* 285: H470–H475, 2003.
26. **Yasuda SI, Sugiura S, Kobayakawa N, Fujita H, Yamashita H, Katoh K, Saeki Y, Kaneko H, Suda Y, Nagai R, and Sugi H.** A novel method to study contraction characteristics of a single cardiac myocyte using carbon fibers. *Am J Physiol Heart Circ Physiol* 281: H1442–H1446, 2001.
27. **Yoneda M.** Force exerted by a single cilium of *Mytilus edulus*. I. *Exp Biol* 37: 461–468, 1960.